

Journal of Sedimentary Research

PETROLOGY OF BENGAL FAN TURBIDITES (IODP EXPEDITIONS 353 AND 354): PROVENANCE VERSUS DIAGENETIC CONTROL

--Manuscript Draft--

Manuscript Number:	2022.071R3
Article Type:	Research Article
Corresponding Author:	Mara Limonta University of Milano–Bicocca: Università degli Studi di Milano-Bicocca Milano, ITALY
First Author:	Mara Limonta
Order of Authors:	Mara Limonta Eduardo Garzanti Alberto Resentini
Abstract:	<p>High-resolution petrographic and heavy-mineral analyses of Bengal Fan turbidites from six cores drilled during IODP Expeditions 353 and 354 elucidate factors controlling their intersample compositional variability as a key to understanding sedimentary processes and erosional evolution of the Himalayan belt since the Miocene. Bengal Fan turbidites are feldspatho-quartzose to litho-feldspatho-quartzose with plagioclase > K-feldspar; slow-settling micas increase in abundance in very fine sand and coarse silt. The feldspar/quartz ratio and higher-rank metamorphic rock fragments notably increase from uppermost Miocene to Pleistocene deposits, which is ascribed to the onset of rapid exhumation of the Eastern Himalayan syntaxis since ~ 5 Ma. The same trends are documented in Nicobar Fan turbidites, confirming that they belong to the same sedimentary system. Both Bengal and Nicobar fans record a pulse in mass accumulation rate at Tortonian times, when supply of sedimentary and very-low-grade metasedimentary detritus reflected accelerated exhumation of the Lesser Himalaya. In contrast to foreland-basin sediments, where ferromagnesian minerals have been completely dissolved in strata as young as Pliocene-Pleistocene, in both Bengal-Nicobar and Indus fans amphibole invariably represents about half of the moderately rich to rich transparent-heavy-mineral suite, demonstrating that amphibolite-facies Greater Himalaya metamorphic rocks were widely exposed in the Himalayan range well before the Late Miocene and possibly since the Late Oligocene, as indicated by a few sillimanite and kyanite grains in Bengal Fan sediments as old as 23 Ma and 28 Ma, respectively. Diagenetic dissolution strongly affected olivine and pyroxene in strata older than the Middle and Early Pleistocene, respectively, whereas amphibole decreases markedly through progressively older Miocene strata. Ferromagnesian minerals and sillimanite are almost completely dissolved in Lower Miocene strata, where durable zircon, tourmaline, rutile, and apatite make up half of the strongly depleted heavy-mineral assemblage. Quaternary turbidites from the six studied cores have virtually the same compositional signatures, testifying to efficient homogenization by turbidite transport and reworking across the fan. Turbidites in western cores closer to peninsular India (U1444A and U1454B) are not different from those in eastern cores, indicating very minor supply from the subcontinent. Forward-mixing calculations based on integrated petrographic and heavy-mineral data indicate that sand supply from the Brahmaputra River to Quaternary turbidites was four times larger than supply from the Ganga River, indicating up to six times higher sediment yields and erosion rates in the Brahmaputra than in the Ganga catchment, largely reflecting superfast erosion of the Eastern Himalayan syntaxis.</p>

Petrology of Bengal Fan turbidites (IODP Expeditions 353 and 354): provenance versus diagenetic control

Mara Limonta^{1,2*}, Eduardo Garzanti^{1*}, Alberto Resentini¹

¹ Laboratory for Provenance Studies, Department of Earth and Environmental Sciences, University of Milano-Bicocca, 20126 Milano, Italy

² Centre de Recherches Péetrographiques et Géochimiques, Université de Lorraine-CNRS, 54501 Vandœuvre-lès-Nancy, France

Emails: mara.limonta@univ-lorraine.fr (Limonta), eduardo.garzanti@unimib.it (Garzanti), alberto.resentini@unimib.it (Resentini)

* Corresponding authors

Keywords: Provenance analysis; Diagenetic dissolution; Sedimentary petrology; Heavy minerals; Miocene-Quaternary; Bengal and Nicobar fans; Brahmaputra and Ganga Rivers; Lesser and Greater Himalaya; Eastern Himalayan Syntaxis

ABSTRACT: High-resolution petrographic and heavy-mineral analyses of Bengal Fan turbidites from six cores drilled during IODP Expeditions 353 and 354 elucidate factors controlling their intersample compositional variability as a key to understanding sedimentary processes and erosional evolution of the Himalayan belt since the Miocene. Bengal Fan turbidites are feldspatho-quartzose to litho-feldspatho-quartzose with plagioclase > K-feldspar; slow-settling micas increase in abundance in very fine sand and coarse silt. The feldspar/quartz ratio and higher-rank metamorphic rock fragments notably increase from uppermost Miocene to Pleistocene deposits, which is ascribed to the onset of rapid exhumation of the Eastern Himalayan syntaxis since ~ 5 Ma. The same trends are documented in Nicobar Fan turbidites, confirming that they belong to the same sedimentary system. Both Bengal and Nicobar fans record a pulse in mass accumulation rate at Tortonian times, when supply of sedimentary and very-low-grade metasedimentary detritus reflected accelerated exhumation of the Lesser Himalaya. In contrast to foreland-basin sediments, where ferromagnesian minerals have been completely dissolved in strata as young as Pliocene-Pleistocene, in both Bengal-Nicobar and Indus fans amphibole invariably represents about half of the moderately rich to rich transparent-heavy-mineral suite, demonstrating that amphibolite-facies Greater Himalaya metamorphic rocks were widely exposed in the Himalayan range well before the Late Miocene and possibly since the Late Oligocene, as indicated by a few sillimanite and kyanite grains in Bengal Fan sediments as old as 23 Ma and 28 Ma, respectively. Diagenetic dissolution strongly affected olivine and pyroxene in strata older than the Middle and Early Pleistocene, respectively, whereas amphibole decreases markedly through progressively older Miocene strata. Ferromagnesian minerals and sillimanite are almost completely dissolved in Lower Miocene strata, where durable zircon, tourmaline, rutile, and apatite make up half of the strongly depleted heavy-mineral assemblage. Quaternary turbidites from the six studied cores have virtually the same compositional signatures, testifying to efficient homogenization by turbidite transport and reworking across the fan. Turbidites in western cores closer to peninsular India (U1444A and U1454B) are not different from those in eastern cores, indicating very minor supply from the subcontinent. Forward-mixing calculations

based on integrated petrographic and heavy-mineral data indicate that sand supply from the Brahmaputra River to Quaternary turbidites was four times larger than supply from the Ganga River, indicating up to six times higher sediment yields and erosion rates in the Brahmaputra than in the Ganga catchment, largely reflecting superfast erosion of the Eastern Himalayan syntaxis.

INTRODUCTION

The Himalayan mountain range is the archetype of orogenic belts produced by continental collision (Hodges 2000). Ongoing indentation between the Indian and Asian continents since ~ 60 Ma (Hu et al. 2016; An et al. 2021) has resulted in accelerated rock uplift associated with rapid exhumation of crystalline basement since the Neogene, and extreme relief and erosion rates around the Eastern Himalayan syntaxis drained by the Brahmaputra River (Zeitler et al. 2001; Booth et al. 2009; Govin et al. 2020). Crucial information for a better understanding of the tectonic growth and erosional evolution of such a complex orogenic region, where geological processes are so intense, is provided by provenance analysis of detritus stored in the Bengal and Nicobar fans, recently cored during three International Ocean Discovery Program (IODP) expeditions: Expedition 353 to the Mahanadi Basin offshore of the Indian coast, the Andaman Islands and the northern Ninety East Ridge (5° N to 20° N; Clemens et al. 2016); Expedition 354 to the middle Bengal Fan along a 320-km-long, east-west transect between the Eighty Five East and Ninety East ridges (~ 8° N; France-Lanord et al. 2016); and Expedition 362 to the proximal Nicobar Fan east of the Ninety East Ridge (~3°N; Dugan et al. 2017).

In the last decades, the mineralogical and geochemical signatures of Ganga and Brahmaputra sediments have been defined in detail (e.g., Galy et al. 2007; Garzanti et al. 2010, 2011; Lupker et al. 2011, 2012). These distinguishing fingerprints can be used to assess the relative sediment supply from the Ganga and Brahmaputra rivers during evolution of the Himalayan belt, also in relationship with intensification of the South Asian Monsoon (Lenard et al. 2020). The composition of Bengal shelf

sediments has also been studied in detail in terms of petrography, mineralogy, and geochemistry (Lupker et al. 2013; Garzanti et al. 2019).

Compositional signatures of Miocene and younger turbidites of Himalayan provenance recovered during IODP Expedition 354 provide insight on how the interplay between tectonics and climate has driven landscape changes across vast continental areas in the past (e.g., Blum et al. 2018; Najman et al. 2019; Huyghe et al. 2020; Lenard et al. 2020). Reconstruction of older geological events is more uncertain because of an increasing number of unknowns, including progressive changes in the tectonic structure of the orogen by subsequent accretion and exhumation of diverse geological units and repeated modifications of drainage systems (e.g., Govin et al. 2018; Zhang et al. 2019). Moreover, the composition of ancient siliciclastic strata is affected by progressively more intense diagenetic dissolution of less durable detrital components during burial diagenesis (Morton and Hallsworth 2007; Andò et al. 2012).

This article focuses on the Bengal Fan sedimentary succession sampled during IODP Expeditions 353 and 354, which extended the record of early fan deposition by 10 Ma into the Upper Oligocene (Fig. 1A). Expedition 354 was designed to: a) provide a spatial overview of the turbiditic depositional system; b) document lateral shifts of depocenters on millennial timescales; and c) reconstruct patterns of Himalayan erosion and the interplay of climate and tectonic activity during long-term and short-term fluctuations of the Indian monsoon. To contribute to these goals, we carried out petrographic and heavy-mineral analyses of 46 turbiditic layers overall, from five short cores covering the terrigenous record over the last 1-2 Ma (Sites U1444, U1454, U1453, U1452, and U1449), and one long core drilled through the complete fan succession reaching the mid-Oligocene (28 Ma; Site U1451) in the middle Bengal Fan.

The main aims of this study are to: a) characterize the compositional variability of Bengal Fan turbidites in space and time through high-resolution petrographic and mineralogical analyses; b) discriminate the relative Ganga *versus* Brahmaputra supply; c) extract information on paleodrainage evolution of the Ganga-Brahmaputra river system in parallel with evolution of the Himalayan

collisional belt; d) compare compositional trends documented in Neogene-Quaternary deep-water successions of the Bengal Fan, Nicobar Fan, and Indus Fan; and e) acquire complementary data to constrain erosion patterns and timing of exhumation of distinct metamorphic domains (e.g., Greater Himalaya, Lesser Himalaya, and Eastern Himalayan syntaxis).

THE GANGA-BRAHMAPUTRA-BENGAL SEDIMENTARY SYSTEM

The modern Ganga and Brahmaputra rivers have a total drainage area of ~ 1.7 million km², including two-thirds of the high-relief Himalayan Range, the southern part of the Tibetan Plateau, and the northern part of the Indian Shield. Their monsoon-driven water discharge is fueled by 1–3 m of annual precipitation in the Ganga, Brahmaputra, and Meghna basins (Mirza 2003). The total annual sediment flux delivered to the Bangladesh delta plain and Bengal Sea is estimated to be 35-40% derived from the Ganga (610 ± 230 million tons) and 60-65% from the Brahmaputra (780–1430 million tons; Lupker et al. 2012; 2017). Erosion rates closely follow precipitation patterns. They are low in the dry Tethys Himalaya and increase with increasing monsoonal precipitation southward and eastward as Ganga and Brahmaputra tributaries cut through the Greater and Lesser Himalaya (Lavé and Avouac 2001; Gabet et al. 2008). Both tectonic and climatic forcing are strong in the Himalayan Range, driving production and transfer of large volumes of sediment to the foreland basin, the delta, and the ocean (Graham et al. 1975; Milliman and Meade 1983; Einsele et al. 1996; Galy and France-Lanord 2001; Clift 2017).

The Brahmaputra and Ganga Rivers

The Yarlung River, representing the Tibetan headwaters of the Brahmaputra, flows along the Transhimalayan suture zone between the Lhasa Block in the north and the Himalayan belt in the south. Detritus is thus derived from the Gangdese arc batholith, forearc ophiolites and siliciclastic

rocks, and Himalayan metamorphic basement and sedimentary strata (Gansser 1980; Zhu et al. 2011; An et al. 2017; Wang et al. 2017). The river plunges into steep gorges across the Eastern Himalayan syntaxis, where 45-60% of the sediment load is generated despite this region encompassing only ~ 20% of the mountain area (Singh and France-Lanord 2002; Enkelmann et al. 2011). The rest of the detritus is provided largely by eastern tributaries draining the Lohit Plutonic Complex, and subordinately by the Himalayan belt, Precambrian granitoid gneisses of the Shillong Plateau, and turbidites of the Indo-Burman Ranges and the Tibetan Plateau (Garzanti et al. 2004).

The Ganga River drains the entire Himalayan orogen and the northern part of the Indian Shield in peninsular India (Upadhyay et al. 2015; Godin et al. 2019), but none of its tributaries reach as far north as the suture zone. Detritus is derived from Paleozoic and Mesozoic sedimentary rocks of the Tethys Himalaya (Garzanti 1999; Sciunnach and Garzanti 2012), amphibolite-facies metamorphic rocks of the Greater Himalaya (Carosi et al. 2019), Proterozoic gneisses and mostly low-grade metasedimentary rocks of the Lesser Himalaya overlain by upper Paleozoic–Cenozoic strata, and Cenozoic foreland-basin sediments of the Subhimalaya (DeCelles et al. 2001, 2004; Najman 2006) (Fig. 1B).

The Bengal Estuary and Shelf

The Ganga and Brahmaputra rivers joined two centuries ago to form the Meghna Estuary, together with the Meghna River sourced in the Indo-Burman Ranges and draining the Shillong Plateau and Bangladesh lowlands (Goodbred et al. 2014). Total annual water and sediment fluxes of ~ 970 km³ and ~ 1.7 billion tons are delivered by the Meghna Estuary, mostly during the summer monsoon (Milliman and Meade 1983; Goodbred and Kuehl 1999). The suspended load consists of very fine to fine silt entrained close to the surface, passing to coarse sandy silt at depth, and to silty sand close to the channel bottom (Lupker et al. 2011; Borromeo et al. 2019). Detritus is stored partly in the floodplain and partly in the subaqueous delta prograding onto the Bengal shelf (Kuehl et al.

2005). Wide sandy topsets extend down to water depths of ~ 15-30 m about 100 km offshore, passing oceanward to delta-front foresets and to muddy prodelta bottomsets at water depths around 80 m. Shelf sediments are resuspended by storms and tides, transported westward by coastal currents parallel to the delta front toward the Swatch of No Ground canyon (Fig. 1A), and finally released episodically to the Bengal Fan as turbidity currents (Michels et al. 2003; Kudrass et al. 2018).

The Bengal and Nicobar Fans

The Bengal and Nicobar fans form the largest deep-sea turbidite system on Earth, part of which has been offscraped and tectonically accreted to the Indo-Burman Ranges and Andaman-Nicobar Islands in the east (Ingersoll et al. 2003; Curray 2005; Limonta et al. 2017). The Bengal Fan extends across the Bay of Bengal, bordered by the Bengal continental slope to the north, by the eastern India continental slope to the west, and by the Ninety East Ridge to the southeast. The Bengal Fan has a length of ~ 3000 km, a width up to 1430 km, an area of 3 million km², and a sediment volume of 12.5 million km³ (Curray et al. 2002; Schwenk and Spieß 2009). The Nicobar Fan is a 1000-1500 km-long secondary lobe extending east of the Ninety East Ridge (McNeill et al. 2017).

Geological studies of the fan started in the early 1950s, and the name Bengal Fan was established in the early 1970s (Dietz 1953; Curray and Moore 1971). Earlier drilling and seismic explorations were carried out during Deep Sea Drilling Project (DSDP) Leg 22 (Heirtzler et al. 1977), Ocean Drilling Program (ODP) Leg 116 (Cochran 1990), and R/V Sonne Cruises SO93, SO125 (Spiess et al. 1998), SO126, and SO188 (Kudrass et al. 2007). IODP Expedition 354 drill sites are located ~ 1400 km to the south of the shelf margin, where a total turbidite thickness of ~ 4 km accumulated through the Neogene and Quaternary (Fig. 1A). Seismic data and high penetration rate during drilling of Hole U1451B show that unconsolidated sand also occurs in the Middle and Lower Miocene but could not be recovered owing to a different coring technique used for Hole U1451B (Rotary Core Barrel, used for coring harder formations and unable to recover loose sand) and Hole

U1451A (Half-Length Advanced Piston Corer, used to recover sand) (France-Lanord et al. 2016).

The stratigraphy of cores drilled during Expedition 354 indicates that accumulation rates averaged 50–100 m/My in the Late Miocene to Early Pliocene and increased to 200 m/My during the Late Pliocene and Early Pleistocene (France-Lanord et al. 2016). Pickering et al. (2020) suggested that sediment accumulation in both Bengal and Nicobar fans, as in the Himalayan foreland basin (Najman et al. 2009), reached a maximum in the Tortonian (~ 9.5–8 Ma), in association with strengthening of the winter monsoon (Gupta et al. 2015). Numerous efforts have been made to assess the influence of climate change on Neogene and Quaternary fan sedimentation, with specific reference to the variability of monsoonal circulation and alternating glacial and interglacial stages (Schwenk and Spieß 2009; Lupker et al. 2013; Jousain et al. 2016; Weber and Reilly 2018). The complex interplay among tectonics, climate, accumulation rates, and sediment composition is, however, hard to disentangle based on evidence from a limited number of cores within the huge Bengal-Nicobar Fan and in the absence of regional seismic lines running away from the delta. The climatic evidence obtained from the high-resolution stratigraphic record from Ocean Drilling Program cores located offshore of the Oman margin and on the Owen Ridge (ODP Sites 722, 728, 730, and 731) and in the South China Sea (ODP Site 1146) indicates that, following a mid-Miocene climatic optimum, climate variability decreased substantially because of weakening of the summer monsoon after ~ 11 Ma (excepting a warm episode at 10.8–10.7 Ma), followed by a long-term cooling trend between ~ 7 and 5.5 Ma synchronous with the intensification of the winter monsoon (Gupta et al. 2015; Holbourn et al. 2021). The most intense maxima peaked between 5.8 and 5.5 Ma before reversing in the Pliocene (Holbourn et al. 2018). Instead, marine records from the Arabian Sea indicate a major strengthening of summer winds between 10 and 8 Ma (Kroon et al. 1991; Clift et al., 2008; Steinke et al. 2010). A gradual weakening of the South Asian monsoon from 6.2 to 2.8 Ma has been inferred based on the clay-mineral record of the Zhaotong Basin in southwestern China (Li et al. 2019) and on a $\delta^{18}\text{O}$ record from the Himalayan foreland basin in northern India (Sanyal et al. 2005). These long-term variations of monsoonal circulation have been explained by changing global

climate towards cooler conditions and expansion of continental ice through the Pliocene (Prell and Kutzbach 1992), although the role of Tibetan Plateau uplift cannot be excluded (Zheng et al. 2000). In the latest Pleistocene to Holocene, phases of stronger monsoonal circulation were identified based on the study of stalagmites in Oman caves (29–24 ka; Fleitmann et al. 2003), of lacustrine deposits in the Sutlej Valley of the northwestern Himalaya (10–4 ka, Bookhagen et al. 2005), and of marine sediments in the Arabian Sea (Clemens et al. 2003; Chen et al. 2018).

Previous Provenance Studies

Provenance studies of Miocene-Quaternary turbidites based on heavy minerals began with DSDP Leg 22 at Sites 218 (latitude 8° N, central Bengal Fan) and 211 (distal Nicobar Fan) (Thompson 1974), and continued with ODP Leg 116 at Sites 717-719 (1° S, distal Bengal Fan; Yokoyama et al. 1990), and IODP Expeditions 354 on the Bengal Fan (Site U1451, latitude 8° N; Yoshida et al. 2021) and 362 on the proximal Nicobar Fan (Sites U1480 and U1481; Pickering et al. 2020). Petrographic studies have been more limited. Ingersoll and Suczek (1979) analyzed turbidites from DSDP Sites 218 and 211, revealing their homogeneous composition and common source from the Himalayan belt. Data from the proximal Nicobar Fan documented a progressive decrease in sedimentary detritus and corresponding increase of higher-grade metamorphic detritus in the Pliocene-Quaternary (Pickering et al. 2020).

Bengal Fan turbidites have long been shown to bear close mineralogical and isotopic similarities with sediments of the modern Ganga and Brahmaputra rivers (e.g., Bouquillon et al. 1990; Copeland and Harrison 1990; Derry and France-Lanord 1996; Galy et al. 1996). Concentrations of major and trace elements remain relatively constant throughout the Neogene and Quaternary, with most variations ascribed to varying proportions of detritus supplied by diverse Himalayan and Transhimalayan sources (France-Lanord et al. 1993). Detrital thermochronological study of sediment samples collected during IODP Expedition 354 documented rapid exhumation of the Greater

Himalaya since before 17 Ma and onset of extremely rapid exhumation of the Eastern Himalayan syntaxis around 4 Ma (Bouquillon et al. 1990; Copeland and Harrison 1990; Najman et al. 2019). Cosmogenic nuclide concentrations indicated fairly constant erosion rates over the past 6 Ma, suggesting that major climatic changes during the Pliocene to Quaternary did not have a prominent impact on Himalayan erosion patterns and total sediment volume exported from the central and eastern Himalayas (Lenard et al. 2020).

SAMPLING AND ANALYTICAL METHODS

The studied 46 mid-Oligocene to upper Quaternary samples of Bengal Fan turbidites were collected by a combination of APC (Advanced Piston Corer), HLAPC (Half Length APC) and XCB (Extended Core Barrel) systems from six different cores, five of which drilled along the 320-km-long E/W transect targeted by IODP Expedition 354 at $\sim 8^\circ$ N and one drilled in the western part of the fan during IODP Expedition 353 at $\sim 14^\circ$ N (Table 1). Twenty-eight Pleistocene coarse silt to fine sand samples were recovered from short cores at Sites U1444, U1454, U1453, U1452, and U1449, and fourteen Upper Miocene (Tortonian) to Middle Pleistocene (Chibanian) coarse silt to medium sand samples and four mid-Oligocene to Tortonian medium to coarse silt samples from the long core at Site U1451 (Fig. 2; Appendix Tables A1). Grain-size data obtained by wet sieving on all samples are provided in Appendix Table A2).

Framework Petrography

A quartered aliquot of each bulk sample was wet sieved using standard 63 μm and 2000 μm steel sieves. The 63-2000 μm fraction thus obtained was impregnated with araldite, cut into a standard thin section, and analyzed by counting 400 points under the petrographic microscope (Gazzi-Dickinson method; Ingersoll et al. 1984; Zuffa 1985). Sand was classified according to the relative abundance of

the three main groups of framework components (Q, quartz; F, feldspar; L, lithic fragments), if exceeding 10% QFL (e.g., in a litho-feldspatho-quartzose sand $Q > F > L > 10\%QFL$; classification scheme after Garzanti 2019a). Petrographic parameters used in this study include the Q/F, P/F and Mic*/F ratios (P, plagioclase, Mic*, microcline with cross-hatched twinning). Low-rank metamorphic lithics were subdivided into metasedimentary and metavolcanic categories, and higher-rank metamorphic lithics into felsic (metapelite, metapsammite, metafelsite) and mafic (metabasite) categories. The average rank of rock fragments is expressed by the Metamorphic Indices MI and MI*: MI varies from 0 (in detritus shed by exclusively sedimentary and volcanic cover rocks) to 500 (in very-high-rank detritus shed by exclusively high-grade basement rocks), whereas MI* considers only metamorphic rock fragments and thus varies from 100 (in very-low-rank detritus shed by exclusively very low-grade metamorphic rocks) to 500 (Garzanti and Vezzoli 2003). Median grain size was determined in thin section by ranking all samples from coarsest to finest, followed by visual comparison with in-house standards prepared at 0.25 ϕ sieve intervals. The complete petrographic dataset is provided in Appendix Table A3.

Heavy Minerals

A quartered aliquot of each bulk sample was wet sieved using a standard 500 μm steel sieve and a 15 μm (sand and coarser silt samples) or 5 μm nylon-mesh sieve (finer silt samples). Such 5 ϕ - to \sim 7 ϕ -wide grain-size windows allowed us to encompass more than 80% of the grain-size distribution for most samples (Appendix Table A4). The dense fraction was separated by centrifuging in Na-polytungstate (density 2.90 g/cm³) and recovered by partial freezing with liquid nitrogen following Andò (2020). Heavy minerals were point-counted under the microscope at a suitable regular spacing (100 μm for most samples) to minimize overestimation of smaller grains (Garzanti and Andò 2019). All dubious grains were systematically checked by Raman spectroscopy. Transparent heavy-mineral assemblages (tHM suites) do not include opaques, alterites,

phyllosilicates, sulfates, and carbonates. According to the transparent-heavy-mineral concentration (tHMC; Garzanti and Andò 2007), tHM suites were defined as poor ($tHMC < 1$), moderately poor ($1 < tHMC < 2$), moderately rich ($2 < tHMC < 5$), and rich ($5 < tHMC < 10$).

The ZTR index (sum of zircon, tourmaline, and rutile over total tHM; Hubert 1962) expresses the durability of the tHM suite through multiple sedimentary cycles (Garzanti 2017). The Amphibole Color Index (ACI) varies from 0 in detritus from low-grade metamorphic rocks yielding exclusively blue/green amphibole to 100 in detritus from granulite-facies or volcanic rocks yielding exclusively brown amphibole or oxy-hornblende (Andò et al. 2014). Among epidote-group minerals, iron-rich epidote *s.s.*, clinozoisite, zoisite, and allanite grains were distinguished based on optical properties and Raman spectra (Limonta et al. 2022). The complete heavy-mineral dataset is provided in Appendix Table A4. Petrographic and heavy-mineral data are illustrated by means of the compositional biplot (Gabriel 1971), which displays the relationships among both multivariate observations (points) and mineralogical variables (rays). The length of each ray is proportional to the variability of the parameter in the data set. The angle between two rays is 0° , 90° , and 180° if the corresponding parameters are correlated, uncorrelated, or inversely correlated, respectively.

PETROGRAPHY AND HEAVY MINERALS

In this section, we illustrate the petrographic composition (Fig. 3) and distribution of heavy minerals (Fig. 4) in the studied Bengal Fan turbidites. Significant minerals are listed in order of abundance (high to low) throughout the text (most/dominant if $> 50\%tHM$, minor if $\leq 5\%tHM$, rare if $\leq 1\%tHM$).

Sand Petrography

Bengal Fan turbidites are mostly feldspatho-quartzose to litho-feldspatho-quartzose, with plagioclase > K-feldspar (Fig. 5A, 5B). Sedimentary and low-rank metasedimentary lithics (siltstone/metasiltstone, phyllite, carbonate; Fig. 3D) decrease in younger beds, whereas high-rank metamorphic lithics increase (schists, gneiss, prasinite, amphibolite, Fig. 3A, 3B). Ultramafic lithics sporadically occur. Mica (biotite > muscovite) sharply increases in finer-grained samples (Fig. 3C). Although the studied samples are petrographically similar overall, significant stratigraphic trends can be detected. Specifically, both plagioclase and K-feldspar tend to increase up-section relative to quartz. The MI and MI* indices also increase, indicating progressive unroofing of higher-grade metamorphic rocks.

Heavy Minerals

The analyzed 35 coarse silt to medium sand turbidites of Quaternary age from Sites U1444A, U1454B, U1453A, U1452B, U1449A, and U1451A yielded mostly moderately rich to rich amphibole-dominated tHM suites with epidote-group minerals, garnet, and minor clinopyroxene, apatite, titanite, sillimanite, tourmaline, zircon, and kyanite (Fig. 5C, 5D). Rutile, staurolite, olivine, green-pink hypersthene, and chloritoid are rare (Fig. 4A, 4B).

Amphibole is mostly blue-green and subordinate green-brown hornblende with minor actinolite (ACI 10 ± 5). Clinopyroxene is mostly diopside, suggesting provenance from high-grade metamorphic rocks of the Eastern Himalayan syntaxis or upper part of the Greater Himalaya sequence (Garzanti et al. 2004, 2007). Garnet is mostly almandine-rich with spessartine, minor grossular, and rare andradite and pyrope. Epidote-group minerals include mainly Fe-rich epidote with subordinate clinozoisite and rare zoisite and allanite.

Among the 11 studied samples from the deep-penetrating core at Site U1451, coarse silt of Zanclean age contains a moderately poor tHM suite with amphibole, epidote, garnet, tourmaline, apatite, minor titanite, zircon, sillimanite, rutile, and rare kyanite and chloritoid (Fig. 4C). A coarse

silt and a very fine sand of Tortonian-Messinian age contain a moderately poor tHM suite with amphibole, epidote, garnet, tourmaline, and minor apatite, titanite, sillimanite, kyanite, staurolite, and zircon (Fig. 4D). Clinopyroxene, chloritoid, and rutile are rare. Four medium to coarse silts and a very fine sand of Tortonian age contain a moderately poor tHM suite with amphibole (including green-brown hornblende and rare oxy-hornblende), epidote, garnet, tourmaline, and minor apatite, zircon, titanite, sillimanite, rutile, clinopyroxene, and kyanite. Chloritoid, staurolite, green-pink hypersthene, and Cr-spinel are rare.

The three oldest analyzed samples from Site U1451B are a silt injectite within mid-Oligocene limestone at the base of the fan, a coarse silt of Aquitanian age, and a medium silt of Burdigalian age. These three samples contain a poor tHM suite with decreasing concentration downcore, including tourmaline, epidote-group minerals, garnet, apatite, zircon, minor rutile and titanite, and rare kyanite and staurolite (Fig. 4E). Amphibole and sillimanite were not detected in the oldest sample, whereas one actinolite grain and one fibrolite grain were identified in the Aquitanian sample and one hornblende grain in the Burdigalian sample. Grandite garnets were not detected in the Aquitanian sample.

ANALYSIS OF INTERSAMPLE MINERALOGICAL VARIABILITY

Compositional variability has diverse controls, including provenance, grain size, weathering, hydraulic sorting, and diagenesis (Garzanti 2016). These superposed effects must be disentangled to obtain information on sedimentary processes and single out the provenance signal. Because selective dissolution of less durable heavy minerals is generally prominent in deeply buried strata, we focused our attention on Pleistocene sediment samples obtained from Sites U1454, U1453, U1452, and U1449 (24 samples; burial depth < 210 m, age < 2 Ma) and from the upper part of Site U1451 (7 samples; burial depth < 120 m, age < 2.5 Ma), for which diagenetic effects can be considered as largely negligible. The compositional variability associated with grain-size and hydrodynamic effects, as

well as the intercore variability is evaluated in this section, whereas the following section is dedicated to diagenetic control. After all factors potentially controlling compositional variability are thoroughly evaluated, provenance information can be obtained from temporal and spatial variation of detrital modes in order to reconstruct the erosional evolution of the Himalayan orogen, understand the interplay between tectonic and climatic agents, and evaluate the variation in relative supply from the Ganga *versus* Brahmaputra rivers and from different geological units and tectono-stratigraphic levels (i.e., Subhimalaya, Lesser Himalaya, Greater Himalaya, Tethys Himalaya, Eastern Himalayan syntaxis, and Transhimalayan arc-trench system).

Grain-Size Control

Mica (biotite > muscovite) sharply increases in finer-grained turbidites, accounting for more than a third of detrital grains in sample 54A27 (Fig. 3C); the concentration of phyllosilicates in finer samples is evident also in heavy-mineral separates. In contrast, both K-feldspar and plagioclase increase relative to quartz in coarser samples (corr. coeff. ~ 0.5 , sign. lev. 1%), together with metabasite lithics and the MI and MI* indices. Because grain size tends to increase up-section, and the feldspar/quartz ratio is generally observed to decrease with grain size (Odom et al. 1976; Garzanti et al. 2021), these trends are considered as related to provenance rather than grain size (see discussion below). Heavy-mineral concentration increases in coarser samples with higher garnet and lower tourmaline content, whereas epidote tends to increase in finer-grained samples.

Hydrodynamic Effects

Hydraulic-sorting effects (Komar 2007; Garzanti et al. 2008, 2009) can be properly investigated only in Quaternary turbidites, where diagenetic effects can be considered as negligible. The highest heavy-mineral concentrations are observed at Site U1454, where tHMC reaches 12 in

sample 54B6 that also contains the most ultradense zircon and opaque Fe-Ti-Cr oxides. The other two samples with rich tHM suites (54B4 and 54B25) also contain higher-than-average amounts of opaque Fe-Ti-Cr oxides. Rich tHM suites also occur at Sites U1444 and U1452, whereas sample 52B22 is slightly enriched in garnet. Sample 51A7 from Site U1451 is also relatively rich in garnet together with opaque Fe-Ti-Cr oxides, which may partly be ascribed to its medium sand size. Conversely, sample 53A3 yielded the lowest garnet content, which may be related to silt size and/or cutoff of the fine tail of the size distribution. In summary, with the partial exception of a few samples, not much mineralogical variability can be ascribed to sedimentary processes such as selective entrainment or winnowing by bottom currents.

Intercore Variability

Quaternary samples from the six studied cores show no significant compositional difference, either from north to south or from west to east, intercore variability being notably less than intracore variability. In Middle Pleistocene and younger turbidites, petrographic modes are virtually identical at the more proximal northwestern Site U1444A and at the distal westernmost Site U1454B of the middle Bengal Fan transect (Table 2). Grain size does not change significantly in turbidites from the proximal Site U1444A to the distal Site U1454B. Differences in detrital modes are also hardly significant across the middle Bengal Fan transect from the westernmost Site U1454B to the easternmost Site U1451A. Although heavy-mineral concentration is somewhat higher in the two western sites, U1444A in the north and U1454B in the middle Bengal Fan transect, the tHM suites are quite similar in all cores, with somewhat less diopsidic clinopyroxene in the easternmost Site U1451A (Table 2). Rather homogeneous tHM suites across the middle Bengal Fan transect indicate minor to negligible supply from the Indian subcontinent, although a few green to brown augite grains occur somewhat more commonly in western Sites U1444A and U1454B. The limited intercore compositional differences testify to the efficient homogenization of detritus supplied by rivers to the

Bay of Bengal, first during remobilization by waves and currents on the shelf and during along-shelf transport towards the Swath of No Ground (Kudrass et al. 2018), and next during turbidite dispersal and reworking of previously deposited sediment by deep-sea currents in the fan (Weber and Reilly 2018).

DIAGENETIC EFFECTS

This section investigates the compositional modifications caused by selective dissolution of less durable detrital minerals, focusing specifically on the older sediment samples from Site U1451A (burial depth ≥ 160 m, age ≥ 5 Ma). Diagenetic trends with age and burial depth are particularly evident for tHM suites (Fig. 5D), whereas petrographic modes are not equally affected (Fig. 5B).

In strata older than Pleistocene, heavy-mineral concentration progressively decreases and the ZTR index and apatite relatively increase with depth at the expense of amphibole and pyroxene (Fig. 4; sign. lev. 1‰). Olivine was never observed in samples older than Middle Pleistocene. Detrital minerals can thus be classified according to their order of durability (Fig. 6): zircon, tourmaline, rutile, apatite, Cr-spinel > epidote, garnet, staurolite > titanite, kyanite > amphibole, sillimanite > pyroxene > olivine. Such a durability order, virtually the same as observed in sedimentary basins worldwide (e.g., Milliken 2007; Morton and Hallsworth 2007; Figure 7 in Garzanti and Andò 2019), indicates that tHM suites are controlled mainly by selective chemical breakdown rather than by provenance. A sequence of diagenetic minerofacies with age and depth (*sensu* Garzanti et al. 2018) can thus be defined. Minerofacies 0, identified in Middle Pleistocene and younger samples (burial depth ≤ 100 m; ZTR 2-10), represents virtually unmodified sediment still containing about the original amount of labile ferromagnesian minerals. Minerofacies 1 (*hornblende zone*), identified in Lower Pleistocene samples (burial depth 150-200 m; ZTR 3-14), represents only slightly modified sediment still containing abundant amphibole and common pyroxene in unchanged proportion, but lacking olivine (Fig. 3). Minerofacies 2 (*epidote-hornblende zone*) characterized by a decrease of the

tHMC index by a factor of 2 in Zanclean to upper Tortonian strata (burial depth down to ~ 450 m; ZTR 5-21) and by a factor of ~ 5 in lower Tortonian strata (burial depth 550-650 m; ZTR 7-24), testifies to the progressive disappearance of ferromagnesian inosilicates, pyroxene faster than amphibole (Table 2). Minerofacies 3 (*epidote-garnet zone*), identified in Lower Miocene samples (burial depth ~ 1000 m) marks a sharp increase in ZTR index (33-40) and apatite (14-16%tHM), and almost complete disappearance of hornblende, pyroxene, and sillimanite (Fig. 6).

Comparison with Indus and Nicobar Fans

The sequence of diagenetic minerofacies observed at Site U1451 compares well with those documented in the Nicobar Fan (Sites U1480 and U1481, Dugan et al. 2017) and Indus Fan (Sites U1456 and U1457, Pandey et al. 2016) (Fig. 7), as with other sedimentary successions worldwide. The selective dissolution of most labile ferromagnesian minerals, defining the transition to minerofacies 1, begins already at very shallow burial depths (≤ 100 m). The breakdown of amphibole, defining the transition to minerofacies 2, starts in Pleistocene strata in the Bengal Fan (burial depth 150-200 m), in Pliocene strata in the Nicobar Fan (burial depth 400-450 m) and Nile Cone (burial depth ~ 500 m), but only in strata older than the Messinian in the Indus Fan (burial depth ~ 800 m). The disappearance of amphibole with relative increase in durable minerals, defining the transition to minerofacies 3, is recorded below the Upper Miocene in the Bengal Fan (burial depth 700-900 m) and below the mid-Miocene in the Indus Fan (burial depth 1100 m). In the Nile Cone it occurs already in Lower Pliocene strata (burial depth ~ 700 m, Garzanti et al. 2018), whereas in the Nicobar Fan it is not recorded in Tortonian strata down to a burial depth of 1350 m.

The disappearance of epidote, indicating the transition to minerofacies 4, is not documented in IODP cores of the Indus, Bengal, and Nicobar fans down to burial depths of 1100-1350 m. In the central North Sea, it is recorded in Paleocene/Eocene strata buried ~ 1100 m (Morton and Hallsworth 2007), in the Nile Cone in Burdigalian strata buried ~ 1350 m (Garzanti et al. 2018), in the Bengal

Basin in Miocene strata buried ~ 2500 m (Andò et al. 2012), and in the Louisiana shelf in sediments as young as Pliocene buried ~ 3000 m (Milliken 2007).

Our data from Site U1451, compared with observations from sedimentary basins worldwide, indicate that diagenetic dissolution during burial is controlled by diverse interplaying factors, including porosity and permeability, geothermal gradient, original sediment mineralogy, and composition of intrastratal fluids. As well documented in the Nile Cone (Garzanti et al. 2018), the similar degree of dissolution observed in Miocene silt and sand from Site U1451 argues against the long-held idea (e.g., Blatt 1985) that unstable minerals are prone to be better preserved in less permeable finer-grained layers.

Geothermal gradients are similar in the Indus Fan (from 53-57°C/km in the upper ~ 100 m of cores U1456 and U1457 to ~ 38°C/km below; Pandey et al. 2016) and Bengal Fan (38°C/km between 100 and 300 m of core U1450A; France-Lanord et al. 2016), as expected for ocean basins of mid-Cretaceous age (e.g., Müller et al. 2008). Geothermal gradients are similar in North Sea basins (30-40 °C/km; Evans and Coleman 1974), but notably lower in the Gulf of Mexico (20-30°C/km; Sharp et al. 1988) and Nile Cone 18-26°C/km; Riad et al. 1989). The greater impact of intrastratal dissolution on Bengal Fan turbidites than on Indus and Nicobar Fan turbidites, therefore, cannot be explained by a difference in geothermal gradient. Nor can differences in sediment mineralogy be invoked, because the Bengal and Nicobar fans belong to the same sedimentary system. As far as fluid circulation and chemistry are concerned, no significant changes have been observed through middle Bengal Fan IODP cores, salinity, alkalinity, and concentration of sulfate, phosphate, potassium, silicon, and magnesium being rather constant between 400 m and 1200 m burial depth (France-Lanord et al. 2016). Several aspects of selective breakdown of labile detrital minerals during diagenesis remain to be investigated.

Weathering versus Diagenesis

Although significant changes in geochemical proxies of silicate breakdown during burial diagenesis have not been reported from the Bengal Fan (France-Lanord et al. 2016), the observed regular trends of heavy-mineral depletion with age and burial depth can hardly be explained by a progressively decreasing intensity of climate-related weathering through time. Ratios of mobile and immobile elements, considered as proxies of chemical weathering, remain stable in Quaternary and Pliocene turbidites and are comparable to modern values (Lupker et al. 2013), and there is no independent indication of weathering conditions extensive and steady enough to explain the markedly regular trend of systematic depletion of progressively less chemically labile minerals in more deeply buried Miocene sediments. Rather, Lower Miocene strata show a relative increase of garnet and apatite, which are well known to be durable during diagenesis but can be rapidly destroyed during pedogenesis (Bateman and Catt 2007; Morton and Hallsworth 2007; Figure 9C in Garzanti et al. 2013). Apatite and most markedly garnet are seen to relatively increase in Miocene sandstones of the Bengal Basin buried up to 4 km (Morton and Hallsworth 2007 p. 224-225; Figure 12 in Andò et al. 2012).

A useful mineralogical parameter to discriminate weathering and diagenetic effects is the G/GCSKA ratio [garnet / (garnet + chloritoid + staurolite + kyanite + andalusite + sillimanite)], which decreases very markedly from unweathered (G/GCSKA $70 \pm 20\%$) to strongly weathered (G/GCSKA $< 5\%$) detritus shed from medium-grade metasedimentary rocks (Garzanti et al. 2022 and references therein). In Quaternary sediments throughout the Ganga-Brahmaputra-Bengal sedimentary system, G/GCSKA values remain invariably in the range of relatively unweathered detritus ($71 \pm 7\%$) and tend to increase in Miocene sediments to reach 91% in the Upper Oligocene/Lower Miocene (Table 2). A similar increase is documented in Miocene strata of the Indus and Nicobar Fans (G/GCSKA% from 77 to 82 and from 57 to 79, respectively; Table 2), indicating downcore concentration of garnet (more durable during burial diagenesis) relative to staurolite, kyanite, and sillimanite (more durable in weathering environments). Moreover, calcareous lithics, which are labile during weathering but chemically stable during diagenesis, tend to increase in strata older than 8 Ma in Bengal Fan (Table

2) and particularly in Nicobar Fan samples (Pickering et al. 2020), suggesting that weathering intensity was hardly greater, and rather possibly weaker, during the Miocene.

PROVENANCE IMPLICATIONS

In the above section, we demonstrate how a large part of mineralogical changes with age and burial depth is determined by the selective dissolution of labile detrital minerals during diagenesis. Distinguishing between diagenetic and provenance control is, however, difficult if, as in the Himalayan case (Garzanti 2019b), erosional unroofing of the orogen may lead to increasing supply through time of minerals grown at high temperatures and pressures, which are also the least stable at diagenetic temperatures (Goldich 1938; Velbel 2007).

Ganga vs. Brahmaputra in the Quaternary

Given the homogeneous composition of Bengal Fan turbidites, and the accurate determination of the average mineralogy of Ganga and Brahmaputra sediments (Table 2), the proportional supply from the Ganga and Brahmaputra Rivers to the Bengal Fan can be assessed by simple forward-mixing calculations (Garzanti et al. 2012; Resentini et al. 2017).

Calculations based on integrated petrographic and heavy-mineral data from the 35 studied sediment samples of Quaternary age, which can be considered as negligibly affected by diagenesis, indicate a clear preponderance of the Brahmaputra River across the fan. The Brahmaputra River is calculated to have supplied at least 80% of total Pleistocene Bengal Fan sediment, whereas contributions by the Ganga River did not exceed 15-20%. Because the Ganga catchment (1,016,000 km²) is 1.5 times larger than the Brahmaputra catchment (670,000 km²), our observations would imply that Pleistocene sediment yields and erosion rates were on average ~ 6 times higher in the Brahmaputra than in the Ganga catchment. These estimates agree with Sr and Nd isotopic signatures

of Quaternary turbidites, which indicate dominant Brahmaputra supply with a Ganga contribution to Meghna Estuary sand of less than 18% (Lenard et al. 2020).

Today, the Brahmaputra sediment load is estimated to be not more than twice that of the Ganga, with average annual sediment yields and erosion rates less than 3 times higher (~ 1650 vs. ~ 600 tons/km² and ~ 0.61 vs. ~ 0.22 mm; Lupker et al. 2012, 2017). A more precise assessment of Quaternary sediment yields and erosion rates would require time-series information on sediment loads through time, which may have varied considerably and reached notably higher values than today during periods of deglaciation or intensified monsoonal rains (up to 2 billion tons per year and perhaps more; Goodbred and Kuehl 2000). Such phases of higher sediment supply should have impacted more heavily the Brahmaputra than the Ganga catchment, considering their present sediment-load ratio.

Compositional Trends Through Time

Provenance changes through time are best revealed by petrographic modes (Fig. 3), which are less affected by diagenesis than heavy-mineral suites. At Site U1451, the quartz/feldspar ratio decreases progressively up-section from Upper Miocene to Lower Pliocene and to Gelasian samples, associated with a slight increase of granitoid and gneissic rock fragments and of metamorphic indices MI and MI*. The increase in higher-rank metamorphic detritus observed after 5 Ma coincides with the sharp decrease in lag time documented by zircon fission-track and rutile U-Pb geochronology between 5.59 and 3.47 Ma. Such a change is ascribed to the onset of extremely rapid exhumation of the Eastern Himalayan syntaxis (Najman et al. 2019), an event that may have initiated at $\sim 4-7$ Ma (Burg et al. 1998; Lang et al. 2016; Govin et al. 2020). Uplift and erosion of Precambrian amphibolite-facies gneisses of the Shillong Plateau, inferred to have taken place since 5-3 Ma (Coutand et al. 2016; Govin et al. 2018), may have also contributed.

Because of the prominent diagenetic effect, heavy-mineral information must be considered with caution. Mild positive correlation among metamorphic rock fragments, MI* indices, garnet

percentage, and ACI index reveals pulses of detritus from higher-grade rocks (e.g., amphibolite and garnet micaschist) that are distributed apparently randomly in space and do not define any apparent trend in time (e.g., Pleistocene samples 51A7 and 53A20, and Tortonian sample 51A66). Kyanite and sillimanite occur in Lower Miocene strata and increase up-section, being significant in Tortonian and younger turbidites. This is notably older than observed in the Siwalik molasse along the front of the Himalayan orogen, where kyanite was reported to appear at 12.2 Ma in northwestern India, at ~ 11 Ma in western Nepal, at 7 Ma in central Nepal, and at ~ 8 Ma in northeastern India, and sillimanite at 7.7 Ma in northwestern India, at ~ 11 Ma in western Nepal, at 7 Ma in central Nepal, and at 7-8 Ma in northeastern India (DeCelles et al. 1998; Szulc et al. 2006; Najman et al. 2009; Vögeli et al. 2018). Such trends are largely diagenetically controlled (Garzanti, 2019b), but heavy-mineral data from the Bengal Fan indicate that amphibolite-facies rocks containing kyanite and sillimanite have been exposed in the Himalaya since the Early Miocene, and extensively since at least the Tortonian. Mostly diopsidic clinopyroxene, largely derived from calcsilicate rocks of the upper Greater Himalaya (Formation II of Colchen et al. 1986; Garzanti et al. 2007) occurs in Gelasian strata. These upper-amphibolite-facies rocks, thus, have been exposed since at least the earliest Pleistocene and very possibly even notably earlier, because diopsidic clinopyroxene may originally have been present in Neogene sediments but subsequently dissolved during burial diagenesis.

Comparison with the Nicobar Fan

Quaternary Bengal Fan and Nicobar Fan turbidites display virtually identical composition, thus confirming that they are part of the same sedimentary system. Older turbidites also share the same composition, but some Nicobar Fan turbidites have more quartz in the Messinian/Pliocene and significant shale fragments in the Tortonian (Table 2). Miocene Nicobar Fan turbidites also contain less plagioclase and show a higher epidote/amphibole ratio, which, however, may be accounted for by diagenesis at greater burial depths (460-1350 m vs. 200 – 660 m at Site U1451). The large influx

of sedimentary to very-low-grade metasedimentary detritus (Fig. 7A), documented also in Bengal Fan turbidites (Fig. 3D), corresponds to a sharp increase in mass accumulation rates recorded at Tortonian times in both Bengal and Nicobar fans (Fig. 2; Pickering et al. 2020). These pieces of evidence combined most plausibly reflect the onset of rapid erosional exhumation of the Lesser Himalaya, starting at 17-16 Ma (White et al. 2002; Myrow et al. 2015; Colleps et al. 2019) and accelerating since ~ 11 Ma (Meigs et al. 1995; Najman et al. 2010; Yoshida et al. 2021).

Comparison with the Indus Fan and Neogene-Quaternary Evolution of the Himalayas

Quaternary Indus Fan turbidites have less quartz, more sedimentary rock fragments (limestone, dolostone, shale/slate, siltstone/metasilstone), and less medium/high-rank metamorphic rock fragments than Quaternary turbidites of the Bengal-Nicobar Fan (Garzanti et al. 2020a). Carbonate detritus supplied from both the Himalayan-Karakorum orogen and the Suleiman-Kirthar Range is preserved across the semiarid Pakistan plains because of dry climate and consequently limited chemical weathering in the floodplain (Garzanti et al. 2005, 2020b; Table 2, Fig. 7A).

In both Bengal–Nicobar and Indus fans, amphibole invariably represents about half of the moderately rich to rich tHM suite throughout Upper Miocene and Quaternary turbidites, in stark contrast to the invariably strongly depleted heavy-mineral suites of the Siwalik molasse deposited all along the Himalayan foreland basin (e.g., Szulc et al. 2006; Najman et al. 2009; Vögeli et al. 2018). This conclusively demonstrates that amphibolite-facies Greater Himalaya metamorphic rocks were widely exposed along the Himalayan Range by the Middle Miocene at least (Yoshida et al. 2021). The Neogene erosional evolution of the Himalaya is, therefore, much more faithfully reflected in the mineralogy of deep-sea sediments than in foreland-basin clastic rocks, which have lost most of the less chemically resistant minerals during diagenesis (Garzanti 2019b).

Although the effective homogenization of sediments prevents us from establishing a detailed chronology of tectonic events affecting specific source areas or geological domains, and to identify

changes in erosion patterns through time, petrographic data clearly show a prominent influx of sedimentary to very-low-grade metasedimentary detritus to both Bengal and Nicobar fans at Tortonian times, followed by a progressive up-section increase of higher-grade metamorphic detritus since 5.0-5.5 Ma (Pickering et al. 2020). The Tortonian event is inferred to reflect accelerated erosional exhumation of the Lesser Himalaya, whereas complementary zircon fission-track and rutile U-Pb geochronological evidence (Najman et al. 2019) indicates that the earliest Pliocene compositional change may testify to the onset of extremely rapid tectonic exhumation of the Eastern Himalayan syntaxis.

CONCLUSIONS

The Bengal Fan, the largest deep-sea cone on Earth, is fed mostly with orogenic detritus supplied by the Brahmaputra and Ganga rivers, and preserves the sedimentary record of the erosional evolution of the Himalayan orogen throughout the Neogene and Quaternary. Bengal Fan turbidites recovered from six cores during IODP Expeditions 353 and 354 at latitudes between 14° N and 8° N have feldspatho-quartzose to litho-feldspatho-quartzose composition, with plagioclase > K-feldspar. Similar compositional trends are documented in the Bengal and Nicobar fans, which both recorded a pulse in mass accumulation rate at Tortonian times, when supply of sedimentary and very-low-grade metasedimentary detritus reflected accelerated exhumation of the Lesser Himalaya. Feldspars and the metamorphic rank of rock fragments increase up-section, plausibly associated with the onset of very rapid exhumation of the Eastern Himalayan syntaxis since the earliest Pliocene (~ 5 Ma).

In both Bengal-Nicobar and Indus fans, the heavy-mineral suites reflect the original detrital assemblage far better than coeval foreland-basin deposits, testifying to extensive exhumation of Greater Himalaya metamorphic rocks well before the Late Miocene. In the deep core at Site U1451, however, heavy-mineral concentration progressively decreases downward through the Neogene (Fig. 4). Olivine and pyroxene have been selectively leached out in strata older than Middle and Early

Pleistocene, respectively, whereas amphibole has been progressively leached out downward in Miocene strata. Lower Miocene strata are relatively enriched in durable ZTR minerals and apatite, but a few sillimanite and kyanite grains still occur in silt as old as 23 Ma and 28 Ma respectively, indicating that amphibolite-facies Greater Himalaya metamorphic rocks may have been exposed in the Himalayan range since as early as the Late Oligocene.

The remarkable homogeneity of petrographic and heavy-mineral signatures in Quaternary samples from the six studied cores indicate efficient homogenization throughout the sedimentary system and by turbidite transport and reworking in the fan. Integrated petrographic and heavy-mineral data show a clear prevalence in sediment supply from the Brahmaputra (80–85%) over the Ganga, which implies up to 6 times higher average sediment yield and erosion rate in the Brahmaputra catchment, explained by very fast exhumation and erosion of the Eastern Himalayan syntaxis since the Early Pliocene.

SUPPLEMENTAL MATERIAL

The supplemental data associated with this article are available from <https://www.sepm.org/supplemental-materials> and include information on sampling sites (Table A1), grain size and textural properties (Table A2), and the complete bulk-petrography (Table A3) and heavy-mineral datasets (Table A4).

ACKNOWLEDGMENTS

We warmly thank Christian France-Lanord for sample selection, thoughtful discussion, and valuable advice. The studied samples were obtained thanks to the International Ocean Discovery Program (IODP) and the kind help of Dr. Kubo and the technical staff of IODP Core Repository Kochi Institute for Core Sample Research (<http://www.kochi-core.jp/en/iodp-curation/index.html>). This research

was funded through MUR for ECORD-IODP Italia (<http://www.iodpitalia.cnr.it/index.php/it/opportunita/bandi-cnr-iodp-it/bando-cnr-ecord-iodp-italia-2018>). We warmly thank Editor Kathleen M. Marsaglia, Associate Editor Raymond V. Ingersoll, and Reviewer Yani Najman and an anonymous reviewer for their very careful critical reading and valuable constructive advice.

FIGURE CAPTIONS

Figure 1. Bengal Fan and Himalayan collision orogen. **A)** Location map with studied IODP sites and sediment isopachs; dotted line encircles combined Ganga-Brahmaputra drainage basin. SoNG, Swatch of No Ground. **B)** Geological sketch map of Himalayas (after Garzanti 2019b).

Figure 2. Stratigraphy of studied cores drilled during IODP Expeditions 353 and 354, with petrographic and heavy-mineral compositions. Q, quartz; KF, K-feldspar; P, plagioclase; L, lithic fragments (Lvm, volcanic and low-rank metavolcanic; Lc, carbonate; Lsm, other sedimentary and low-rank metasedimentary; Lmf, high-rank metapelite and metafelsite; Lbu, high-rank metabasite and ultramafic). HM, heavy minerals. ZTR, zircon + tourmaline + rutile; Ap, apatite; Ttn, titanite; Ep, epidote; Grt, garnet; CSKA, chloritoid + staurolite + kyanite + andalusite + sillimanite; Amp, amphibole; Px, pyroxene; &tHM, other transparent heavy minerals.

Figure 3. Petrography of litho-feldspatho-quartzose Bengal Fan turbidites. Quaternary **A)** fine and **B)** medium sands richer in feldspars and high-rank metamorphic lithics. **C)** Abundant mica and foraminifera (*f*) in very fine Lower Pliocene sand. **D)** Predominance of sedimentary and metasedimentary lithics in Upper Miocene sand. Q, quartz; P, plagioclase; L, lithic grain (Lc, carbonate, Lms, low-rank metasedimentary; Lm, high-rank metamorphic; Lv, volcanic); a, amphibole; b, biotite, c, clinozoisite; p, pyroxene; s, sillimanite. All photos with crossed polars. Blue bar for scale 100 μm .

Figure 4. Transparent heavy minerals in Bengal Fan turbidites. **A)** Middle Pleistocene and younger turbidites contain amphibole, epidote, garnet, staurolite, kyanite, sillimanite, and corroded pyroxenes and olivine. **B)** Lower Quaternary strata contain etched pyroxene but no olivine. **C)** Pyroxene is lost in Pliocene turbidites, where transparent-heavy-mineral concentration (tHMC) starts to sharply decrease. **D)** Amphibole grains decrease in Upper Miocene strata, where they appear corroded to various degrees. **E)** The tHMC index decreases further in Lower Miocene strata, where zircon, tourmaline, and apatite relatively increase, garnet is corroded, and amphibole disappears. Blue bar for scale 100 μm .

Figure 5. Intersample mineralogical variability in Bengal Fan turbidites. Sand petrography of: **A)** Quaternary samples from short cores; **B)** Miocene-Pleistocene samples from Site U1451 (depositional ages are indicated). Relative abundance of the three most common heavy-mineral groups in: **C)** Quaternary samples from short cores; **D)** Miocene-Pleistocene samples from Site U1451. Because of different density (amphibole $\sim 3.2 \text{ g/cm}^3$; epidote $\sim 3.45 \text{ g/cm}^3$; garnet $\sim 4.0 \text{ g/cm}^3$) and durability during diagenesis (garnet > epidote > amphibole), relative proportions are controlled mostly by provenance and subordinately by hydraulic sorting in Quaternary turbidites and mostly by diagenesis in older strata.

Figure 6. Diagenetic control on heavy-mineral suites (depositional ages are indicated for Site U1451). Middle Pleistocene and younger turbidites largely preserve their original depositional signature, whereas olivine is lost in Lower Pleistocene sediments, pyroxene in Pliocene sediments, and amphibole and sillimanite in Oligocene silt. Order of mineral durability indicated by biplot is olivine < pyroxene < amphibole \approx sillimanite < kyanite < garnet and other minerals.

Figure 7. Comparison of compositional trends in Bengal, Nicobar, and Indus fans. **A)** Sand petrography is chiefly provenance related. Ganga and Indus sands contain carbonate grains, which are weathered out in Brahmaputra sand. Bengal Fan turbidites (circles) plot between Ganga and Brahmaputra sands, with some samples virtually identical to Brahmaputra sand, Meghna Estuary, and Bengal Shelf sediments. Bengal and Nicobar turbidites share same composition in Quaternary, showing increase in feldspars and higher-rank metamorphic detritus since Pliocene; sedimentary detritus is most abundant in Upper Miocene Nicobar turbidites. **B)** Heavy minerals are strongly affected by diagenetic dissolution: olivine is lost in Lower Pleistocene, pyroxene in Pliocene, and amphibole progressively decreases through Miocene strata where durable minerals relatively increase.

Table 1. Key information on studied cores from IODP Expeditions 353 and 354 (time scale after Cohen et al. 2021).

Table 2. Key petrographic and heavy-mineral parameters for Bengal-Nicobar Fan and Indus Fan turbidites, compared with modern sands from Ganga River, Brahmaputra River, Meghna Estuary, Bengal Shelf, Indus River, and Indus Delta. N^o, number of samples; Q, quartz; KF, K-feldspar; P, plagioclase; L, lithic grains (Lc, carbonate; &Lsm, other sedimentary and low-rank metasedimentary; Lmf, high-rank metamorphic; Lvbu, volcanic, metabasite and ultramafic); MI = Metamorphic Index. HM, heavy-minerals (% in volume); tHMC, transparent heavy-mineral concentration (% over total sample in weight); ZTR, zircon + tourmaline + rutile; Ap, apatite; Ttn, titanite; Ep, epidote-group; Grt, garnet; CSKA, chloritoid + staurolite + kyanite + andalusite + sillimanite; Amp, amphibole; Px, pyroxene; &tHM, other transparent heavy minerals (Cr-spinel, anatase, brookite, monazite, vesuvianite, pumpellyite, prehnite, olivine, diaspore). G/GCSKA, garnet / (garnet + chloritoid + staurolite + kyanite + andalusite + sillimanite) * 100. Data sources: * This study; ° Garzanti et al. (2004, 2005, 2010, 2011, 2019, 2020a); § Clift et al. 2010; # Pickering et al. (2020).

REFERENCES

- An, W., Hu, X., and Garzanti, E., 2017, Sandstone provenance and tectonic evolution of the Xiukang Mélange from Neotethyan subduction to India-Asia collision (Yarlung-Zangbo suture). *Gondwana Research*, v. 41, p. 222–234.
- An, W., Hu, X., Garzanti, E., Wang, J. G., and Liu, Q., 2021, New precise dating of the India - Asia collision in the Tibetan Himalaya at 61 Ma: *Geophysical Research Letters*, v. 48 (3), n° e2020GL090641.
- Andò, S., 2020, Gravimetric separation of heavy minerals in sediments and rocks: *Minerals*, v. 10(3), n°273, doi:10.3390/min10030273.
- Andò, S., Garzanti, E., Padoan, M., and Limonta, M., 2012, Corrosion of heavy minerals during weathering and diagenesis: A catalog for optical analysis: *Sedimentary Geology*, v. 280, p. 165-178.
- Andò, S., Morton, A., and Garzanti, E., 2014, Metamorphic grade of source rocks revealed by chemical fingerprints of detrital amphibole and garnet *in* Scott, R.A., Smyth, H.R., Morton, A.C., and Richardson, N., eds., *Sediment Provenance Studies in Hydrocarbon Exploration and Production: Geological Society of London, Special Publications 386(1)*, p. 351-371.
- Bateman, R.M., and Catt, J.A., 2007. Provenance and palaeoenvironmental interpretation of superficial deposits, with particular reference to post-depositional modification of heavy mineral assemblages, *in* Mange, M.A., and Wright, D.T., eds., *Heavy Minerals in Use: Elsevier, Amsterdam, Developments in Sedimentology*, v. 58, p. 151-188.
- Blatt, H., 1985, Provenance studies and mudrocks: *Journal of Sedimentary Petrology*, v. 55(1), p. 69-75.
- Blum, M., Rogers, K., Gleason, J., Najman, Y., Cruz, J., and Fox, L., 2018, Allogenic and autogenic signals in the stratigraphic record of the deep-sea Bengal Fan: *Scientific Reports*, v. 8(1), p. 1-13.

- Bookhagen, B., Thiede, R. C., and Strecker, M. R., 2005, Late Quaternary intensified monsoon phases control landscape evolution in the northwest Himalaya: *Geology*, v. 33(2), p. 149-152.
- Booth, A.L., Chamberlain, C.P., Kidd, W.S.F., and Zeitler, P.K., 2009, Constraints on the metamorphic evolution of the eastern Himalayan syntaxis from geochronologic and petrologic studies of Namche Barwa: *Geological Society of America, Bulletin*, v. 121, p. 385–407.
- Borromeo, L., Andò, S., France-Lanord, C., Coletti, G., Hahn, A., and Garzanti, E., 2019, Provenance of Bengal shelf sediments: 1. Mineralogy and geochemistry of silt: *Minerals*, v. 9(10), n°640, doi.org/10.3390/min9100640.
- Bouquillon, A., France-Lanord, C., Michard, A., and Tiercelin, J.J., 1990, Sedimentology and Isotopic Chemistry of the Bengal Fan Sediments: The Denudation of the Himalaya, *in* Cochran, J.R., Stow, D.A., et al., eds., *Proceedings of the Ocean Drilling Program, Scientific Results*, v. 116, p. 43–58, doi.org/10.2973/odp.proc.sr.116.117.1990.
- Burg, J.P., Nievergelt, P., Oberli, F., Seward, D., Davy, P., Maurin, J.C., Diao, Z. and Meier, M., 1998, The Namche Barwa syntaxis: evidence for exhumation related to compressional crustal folding: *Journal of Asian Earth Sciences*, v.16(2-3), p. 239-252.
- Carosi, R., Montomoli, C., Iaccarino, S., and Visonà, D., 2019, Structural evolution, metamorphism and melting in the Greater Himalayan Sequence in central-western Nepal *in* Treloar, P.J., and Searle, M.P., eds., *Himalayan Tectonics: A Modern Synthesis*: Geological Society of London, Special Publications 483(1), p. 305-323.
- Chen, H., Xu, Z., Clift, P.D., Lim, D., Khim, B.-K., and Yu, Z., 2018, Orbital-scale evolution of Indian summer monsoon since 1.2 Ma: Evidence from clay mineral records at IODP Exp. 355 Site U1456 in the eastern Arabian Sea. *Journal of Asian Earth Sciences*. Doi:10.1016/j.jseaes.2018.10.012.
- Clemens, S.C., and Prell, W.L., 2003, A 350,000 year summer-monsoon multi-proxy stack from the Owen Ridge, Northern Arabian Sea. *Marine Geology*, v. 201, p. 35-51.

- Clemens, S.C., Kuhnt, W., LeVay, L.J., Anand, P., Ando, T., Bartol, M., Bolton, C.T., Ding, X., Gariboldi, K., Giosan, L., Hathorne, E.C., Huang, Y., Jaiswal, P., Kim, S., Kirkpatrick, J.B., Littler, K., Marino, G., Martinez, P., Naik, D., Peketi, A., Phillips, S.C., Robinson, M.M., Romero, O.E., Sagar, N., Taladay, K.B., Taylor, S.N., Thirumalai, K., Uramoto, G., Usui, Y., Wang, J., Yamamoto, M., and Zhou, L., 2016. Expedition 353 summary, *in* International Ocean Discovery Program 353 Preliminary Report; IODP: College Station, Texas, USA, p. 1-33, doi.org/10.14379/iodp.proc.353.101.2016.
- Clift, P.D., 2017, Cenozoic sedimentary records of climate-tectonic coupling in the Western Himalaya: *Progress in Earth and Planetary Science*, v. 4 (1), p. 1-22.
- Clift, P.D., Giosan, L., Blusztajn, J., Campbell, I.H., Allen, C., Pringle, M., Tabrez, A., Danish, M., Rabbani, M., Alizai, A., Carter, A., and Lückge, A., 2008, Holocene erosion of the Lesser Himalaya triggered by intensified summer monsoon: *Geology*, v. 36 (1), p. 79-82, <https://doi.org/10.1130/G24315A.1>
- Clift, P.D., Giosan, L., Carter, A., Garzanti, E., Galy, V., Tabrez, A.R., Pringle, M., Campbell, I.H., France-Lanord, C., Blusztajn, J., and Allen, C., 2010, Monsoon control over erosion patterns in the western Himalaya: possible feed-back into the tectonic evolution *in* Clift, P.D., Tada, R., and Zheng, H., eds., *Monsoon Evolution and Tectonics–Climate Linkage in Asia*: Geological Society of London, Special Publications 342(1), p.185-218.
- Cochran, J. R., 1990, Himalayan uplift, sea level, and the record of Bengal Fan sedimentation at the ODP Leg 116 sites, *in* Cochran, J.R., Stow, D.A.V., et al., eds., *Proceedings of the Ocean Drilling Program, Scientific Results*, v. 116, p. 397-414.
- Cohen, K.M., Finney, S.C., Gibbard, P.L., and Fan, J.X., 2013, The ICS international chronostratigraphic chart: *Episodes Journal of International Geoscience*, v. 36(3), p. 199-204.
- Colchen, M., Le Fort, P., and Pêcher, A., 1986, Annapurna, Manaslu, Ganesh Himal (with 1:200.000 geological map): Paris, Éditions du Centre national de la recherche scientifique, 136 p.

- Colleps, C.L., Stockli, D.F., McKenzie, N.R., Webb, A.A.G., and Horton, B.K., 2019, Neogene kinematic evolution and exhumation of the NW India Himalaya: Zircon geo- and thermochronometric insights from the fold-thrust belt and foreland basin: *Tectonics*, v. 38(6), p. 2059-2086.
- Copeland, P., and Harrison, T.M., 1990, Episodic rapid uplift in the Himalaya revealed by $^{40}\text{Ar}/^{39}\text{Ar}$ analysis of detrital K-feldspar and muscovite, Bengal fan: *Geology*, v. 18(4), p. 354-357.
- Coutand, I., Barrier, L., Govin, G., Grujic, D., Hoorn, C., Dupont-Nivet, G., and Najman, Y., 2016, Late Miocene - Pleistocene evolution of India-Eurasia convergence partitioning between the Bhutan Himalaya and the Shillong Plateau: New evidences from foreland basin deposits along the Dungsam Chu section, eastern Bhutan: *Tectonics*, v. 35(12), p. 2963-2994.
- Curray, J.R., and Moore, D.G., 1971, Growth of the Bengal deep-sea fan and denudation in the Himalayas: *Geological Society of America, Bulletin*, v. 82(3), p. 563-572.
- Curray, J.R., Emmel, F.J., and Moore, D.G., 2002, The Bengal Fan: morphology, geometry, stratigraphy, history and processes: *Marine and Petroleum Geology*, v. 19(10), p. 1191-1223.
- Curray, J.R., 2005, Tectonics and history of the Andaman Sea region: *Journal of Asian Earth Sciences*, v. 25(1), p. 187-232.
- DeCelles, P.G., Gehrels, G.E., Quade, J., Ojha, T.P., Kapp, P.A., and Upreti, B.N., 1998, Neogene foreland basin deposits, erosional unroofing, and the kinematic history of the Himalayan fold-thrust belt, western Nepal: *Geological Society of America, Bulletin*, v. 110(1), p. 2-21.
- DeCelles, P.G., Robinson, D.M., Quade, J., Ojha, T.P., Garzzone, C.N., Copeland, P., and Upreti, B.N., 2001, Stratigraphy, structure, and tectonic evolution of the Himalayan fold-thrust belt in western Nepal: *Tectonics*, v. 20(4), p. 487-509.
- DeCelles, P.G., Gehrels, G.E., Najman, Y., Martin, A.J., Carter, A., and Garzanti, E., 2004, Detrital geochronology and geochemistry of Cretaceous–Early Miocene strata of Nepal: implications for

timing and diachroneity of initial Himalayan orogenesis: *Earth and Planetary Science Letters*, v. 227(3-4), p. 313-330.

Derry, L.A., and France-Lanord, C., 1996, Neogene Himalayan weathering history and river ^{87}Sr ^{86}Sr : impact on the marine Sr record: *Earth and Planetary Science Letters*, v. 142(1-2), p. 59-74.

Dietz, R.S., 1953, Possible deep-sea turbidity-current channels in the Indian Ocean: *Geological Society of America, Bulletin*, v. 64(3), p. 375-378.

Dugan, B., McNeill, L., Petronotis, K., and the Expedition 362 Scientists, 2017, Expedition 362 Preliminary Report Sumatra Subduction Zone *in* International Ocean Discovery Program 362: College Station, Texas, USA, p. 1-31, doi.org/10.14379/iodp.pr.362.2017.

Einsele, G., Ratschbacher, L., and Wetzel, A., 1996, The Himalaya-Bengal Fan denudation accumulation system during the past 20 Ma: *The Journal of Geology*, v. 104(2), p. 163-184.

Enkelmann, E., Ehlers, T.A., Zeitler, P.K., and Hallet, B., 2011, Denudation of the Namche Barwa antiform, eastern Himalaya. *Earth and Planetary Science Letters*, v. 307 (3), p. 323-333, doi:10.1016/j.epsl.2011.05.004.

Evans, T.R., and Coleman, N.C., 1974, North Sea geothermal gradients: *Nature*, v. 247, p. 28–30.

Fleitmann, D., Burns, S.J., Mudelsee, M., Neff, U., Kramers, J., Mangini, A., and Matter, A., 2003, Holocene forcing of the Indian monsoon recorded in a stalagmite from southern Oman: *Science*, v. 300, p. 1737–1739.

France-Lanord, C., Derry, L., and Michard, A., 1993, Evolution of the Himalaya since Miocene time: isotopic and sedimentological evidence from the Bengal Fan, *in* Treloar, P.J. and Searle, M.P., eds., *Himalayan Tectonics*: Geological Society of London, Special Publications 74(1), p. 603-621.

- France-Lanord, C., Spiess, V., Klaus, A., Schwenk, T., Adhikari, T.T., Adhikari, S.K., Bahk, J.J., Baxter, A.T., Cruz, J.W., Das, S.K., et al., 2016, Expedition 354 summary, *in* International Ocean Discovery Program 354 Preliminary Report; IODP: College Station, Texas, USA, p. 1–35.
- Gabet, E.J., Burbank, D.W., Pratt-Sitaula, B., Putkonen, J., and Bookhagen, B., 2008, Modern erosion rates in the High Himalayas of Nepal: *Earth and Planetary Science Letters*, v. 267(3-4), p. 482-494.
- Gabriel, K.R., 1971, The biplot graphic display of matrices with application to principal component analysis: *Biometrika*, v. 58(3), p.453-467.
- Galy, A., and France-Lanord, C., 2001, Higher erosion rates in the Himalaya: Geochemical constraints on riverine fluxes: *Geology*, v. 29 (1), p. 23-26.
- Galy, A., France-Lanord, C., and Derry, L.A., 1996, The Late Oligocene-Early Miocene Himalayan belt constraints deduced from isotopic compositions of Early Miocene turbidites in the Bengal Fan: *Tectonophysics*, v. 260(1-3), p. 109-118.
- Galy, V., France-Lanord, C., Beyssac, O., Faure, P., Kudrass, H., and Palhol, F., 2007, Efficient organic carbon burial in the Bengal fan sustained by the Himalayan erosional system: *Nature*, v. 450 (7168), p. 407-410.
- Gansser, A., 1980, The Peri-Indian suture zone, in Auboin, J., Debelmas, J., Latreille, M., eds., *Géologie des Chaînes Alpines Issues de la Téthys; Mémoires B.R.G.M.: Paris, France; Volume 115*, p. 140–148.
- Garzanti, E., 1999, Stratigraphy and sedimentary history of the Nepal Tethys Himalaya passive margin: *Journal of Asian Earth Sciences*, v. 17(5-6), p. 805-827.
- Garzanti, E., 2016, From static to dynamic provenance analysis-Sedimentary petrology upgraded. *Sedimentary Geology*, v. 336, p. 3-13.

- Garzanti, E., 2017, The maturity myth in sedimentology and provenance analysis: *Journal of Sedimentary Research*, v. 87(4), p. 353-365.
- Garzanti, E., 2019a, Petrographic classification of sand and sandstone: *Earth-Science Reviews*, v. 192, p. 545-563.
- Garzanti, E., 2019b, The Himalayan Foreland Basin from collision onset to the present: A sedimentary–petrology perspective, *in* Treloar, P.J., and Searle, M.P., eds., *Himalayan Tectonics: A Modern Synthesis*: Geological Society of London, Special Publications 483(1), p. 65-122.
- Garzanti, E., and Andò, S., 2007, Heavy mineral concentration in modern sands: implications for provenance interpretation, *in* Mange, M.A., and Wright, D.T., eds., *Heavy Minerals in Use*: Elsevier, Amsterdam, *Developments in Sedimentology*, v. 58, p. 517-545.
- Garzanti, E., and Andò, S., 2019, Heavy minerals for junior woodchucks: *Minerals*, v. 9(3), n° 148, doi.org/10.3390/min9030148.
- Garzanti, E., and Vezzoli, G., 2003, A classification of metamorphic grains in sands based on their composition and grade: *Journal of Sedimentary Research*, v. 73(5), p. 830-837.
- Garzanti, E., Vezzoli, G., Andò, S., France-Lanord, C., Singh, S.K., and Foster, G., 2004, Sand petrology and focused erosion in collision orogens: the Brahmaputra case: *Earth and Planetary Science Letters*, v. 220(1-2), p. 157-174.
- Garzanti, E., Vezzoli, G., Andò, S., Paparella, P., and Clift, P.D., 2005, Petrology of Indus River sands: a key to interpret erosion history of the Western Himalayan Syntaxis: *Earth and Planetary Science Letters*, v. 229(3-4), p. 287-302.
- Garzanti, E., Vezzoli, G., Andò, S., Lavé, J., Attal, M., France-Lanord, C., and DeCelles, P., 2007, Quantifying sand provenance and erosion (Marsyandi River, Nepal Himalaya): *Earth and Planetary Science Letters*, v. 258(3-4), p. 500-515.

- Garzanti, E., Andò, S., and Vezzoli, G., 2008, Settling equivalence of detrital minerals and grain-size dependence of sediment composition: *Earth and Planetary Science Letters*, v. 273(1-2), p. 138-151.
- Garzanti, E., Andò, S., and Vezzoli, G., 2009, Grain-size dependence of sediment composition and environmental bias in provenance studies: *Earth and Planetary Science Letters*, v. 277(3-4), p. 422-432.
- Garzanti, E., Andò, S., France-Lanord, C., Vezzoli, G., Censi, P., Galy, V., and Najman, Y., 2010, Mineralogical and chemical variability of fluvial sediments: 1. Bedload sand (Ganga–Brahmaputra, Bangladesh): *Earth and Planetary Science Letters*, v. 299(3-4), p. 368-381.
- Garzanti, E., Andò, S., France-Lanord, C., Censi, P., Vignola, P., Galy, V., and Lupker, M., 2011, Mineralogical and chemical variability of fluvial sediments 2. Suspended-load silt (Ganga–Brahmaputra, Bangladesh): *Earth and Planetary Science Letters*, v. 302(1-2), p. 107-120.
- Garzanti, E., Resentini, A., Vezzoli, G., Andò, S., Malusà, M., and Padoan, M., 2012, Forward compositional modelling of Alpine orogenic sediments: *Sedimentary Geology*, v. 280, p. 149-164.
- Garzanti, E., Padoan, M., Andò, S., Resentini, A., Vezzoli, G., and Lustrino, M., 2013, Weathering and relative durability of detrital minerals in equatorial climate: sand petrology and geochemistry in the East African Rift: *The Journal of Geology*, v. 121(6), p. 547-580.
- Garzanti, E., Andò, S., Limonta, M., Fielding, L., and Najman, Y., 2018, Diagenetic control on mineralogical suites in sand, silt, and mud (Cenozoic Nile Delta): Implications for provenance reconstructions: *Earth-Science Reviews*, v. 185, p. 122-139.
- Garzanti, E., Vezzoli, G., Andò, S., Limonta, M., Borromeo, L., and France-Lanord, C., 2019, Provenance of Bengal shelf sediments: 2. Petrology and geochemistry of sand: *Minerals*, v. 9(10), n°642, doi.org/10.3390/min9100642.

- Garzanti, E., Andò, S., and Vezzoli, G., 2020a, Provenance of Cenozoic Indus Fan sediments (IODP Sites U1456 and U1457): *Journal of Sedimentary Research*, v. 90(9), p. 1114-1127.
- Garzanti, E., Liang, W., Andò, S., Clift, P.D., Resentini, A., Vermeesch, P., and Vezzoli, G., 2020b, Provenance of Thal Desert sand: Focused erosion in the western Himalayan syntaxis and foreland-basin deposition driven by latest Quaternary climate change: *Earth-Science Reviews*, v. 207, n°103220, doi.org/10.1016/j.earscirev.2020.103220.
- Garzanti, E., Bayon, G., Dennielou, B., Barbarano, M., Limonta, M., and Vezzoli, G., 2021, The Congo deep-sea fan: Mineralogical, REE, and Nd-isotope variability in quartzose passive-margin sand: *Journal of Sedimentary Research*, v. 91(5), p. 433-450.
- Garzanti, E., Pastore, G., Stone, A., Vainer, S., Vermeesch, P., and Resentini, A., 2022, Provenance of Kalahari Sand: Paleoweathering and recycling in a linked fluvial-aeolian system. *Earth-Science Reviews*, v. 224, n° 103867.
- Godin, L., Soucy La Roche, R., Waffle, L. and Harris, L.B., 2019, Influence of inherited Indian basement faults on the evolution of the Himalayan Orogen, *in*: Sharma, R., Villa, I.M., and Kumar, S., eds., *Crustal Architecture and Evolution of the Himalaya–Karakoram–Tibet Orogen*: Geological Society of London, Special Publications 481, p. 251-266.
- Goldich, S.S., 1938, A study in rock-weathering: *The Journal of Geology*, v. 46(1), p. 17-58.
- Goodbred S.L. Jr, and Kuehl, S.A., 1999, Holocene and modern sediment budgets for the Ganges-Brahmaputra river system: Evidence for highstand dispersal to flood-plain, shelf, and deep-sea depocenters: *Geology*, v. 27(6), p. 559-562.
- Goodbred S.L., Jr, and Kuehl, S.A., 2000, Enormous Ganges-Brahmaputra sediment discharge during strengthened early Holocene monsoon: *Geology*, v. 28(12), p. 1083-1086.
- Goodbred, S.L., Paolo, P.M., Ullah, M.S., Pate, R.D., Khan, S.R., Kuehl, S.A., Singh, S.K., and Rahaman, W., 2014, Piecing together the Ganges-Brahmaputra-Meghna River delta: Use of

sediment provenance to reconstruct the history and interaction of multiple fluvial systems during Holocene delta evolution. *Geological Society of America, Bulletin*, v. 126, p. 1495–1510.

Govin, G., Najman, Y., Copley, A., Millar, I., Van Der Beek, P., Huyghe, P., Grujic, D., and Davenport, J., 2018, Timing and mechanism of the rise of the Shillong Plateau in the Himalayan foreland: *Geology*, v. 46(3), p. 279-282.

Govin, G., Van der Beek, P., Najman, Y., Millar, I., Gemignani, L., Huyghe, P., Dupont-Nivet, G., Bernet, M., Mark, C., and Wijbrans, J., 2020, Early onset and late acceleration of rapid exhumation in the Namche Barwa syntaxis, eastern Himalaya: *Geology*, v. 48(12), p. 1139-1143.

Graham, S.A., Dickinson, W.R., and Ingersoll, R.V., 1975, Himalayan-Bengal model for flysch dispersal in the Appalachian-Ouachita system. *Geological Society of America, Bulletin*, v. 86(3), p. 273-286.

Gupta, A.K., Yuvaraja, A., Prakasam, M., Clemens, S.C., and Velu, A., 2015, Evolution of the South Asian monsoon wind system since the late Middle Miocene. *Palaeogeography, Palaeoclimatology, Palaeoecology*, v. 438, p. 160-167.

Heirtzler, J.R., Bolli H.M., Davies, T.A., Saunders, J.B., and Sclater, J.G., 1977, Indian Ocean Geology and Biostratigraphy: Studies Following Deep-sea Drilling Legs 22-29. American Geophysical Union, Special Publication Series, v. 9, 616 p.

Hodges, K.V., 2000, Tectonics of the Himalaya and southern Tibet from two perspectives: *Geological Society of America, Bulletin*, v. 112(3), p. 324-350.

Holbourn, A. E., Kuhnt, W., Clemens, S. C., Kochhann, K. G., Jöhnck, J., Lübbers, J., and Andersen, N., 2018, Late Miocene climate cooling and intensification of southeast Asian winter monsoon: *Nature communications*, v. 9(1), p. 1584.

- Holbourn, A., Kuhnt, W., Clemens, S. C., and Heslop, D., 2021, A ~ 12 Myr Miocene record of East Asian Monsoon variability from the South China Sea: *Paleoceanography and Paleoclimatology*, v. 36(7), n° e2021PA004267.
- Hu, X., Wang, J., Boudagher-Fadel, M., Garzanti, E., and An, W., 2016, New insights into the timing of the India–Asia collision from the Paleogene Quxia and Jialazi formations of the Xigaze forearc basin, South Tibet: *Gondwana Research*, v. 32, p. 76-92.
- Hubert, J.F., 1962, A zircon-tourmaline-rutile maturity index and the interdependence of the composition of heavy mineral assemblages with the gross composition and texture of sandstones: *Journal of Sedimentary Petrology*, v. 32(3), p. 440-450.
- Huyghe, P., Bernet, M., Galy, A., Naylor, M., Cruz, J., Gyawali, B.R., Gemignani, L., and Mugnier, J.L., 2020, Rapid exhumation since at least 13 Ma in the Himalaya recorded by detrital apatite fission-track dating of Bengal fan (IODP Expedition 354) and modern Himalayan river sediments: *Earth and Planetary Science Letters*, v. 534, n° 116078, doi.org/10.1016/j.epsl.2020.116078.
- Ingersoll, R.V., and Suczek, C.A., 1979, Petrology and provenance of Neogene sand from Nicobar and Bengal fans, DSDP sites 211 and 218: *Journal of Sedimentary Petrology*, v. 49(4), p. 1217-1228.
- Ingersoll, R.V., Bullard, T.F., Ford, R.L., Grimm, J.P., Pickle, J.D., and Sares, S.W., 1984, The effect of grain size on detrital modes: a test of the Gazzi-Dickinson point-counting method: *Journal of Sedimentary Petrology*, v. 54, p. 103-116.
- Ingersoll, R.V., Dickinson, W.R., and Graham, S.A., 2003, Remnant-ocean submarine fans: largest sedimentary systems on Earth, *in* Chan, M.A., and Archer, A.W., eds., *Extreme Depositional Environments: Mega End Members in Geologic Time*: Geological Society of America, Special Paper 370, p. 191-208.

- Joussain, R., Colin, C., Liu, Z., Meynadier, L., Fournier, L., Fauquembergue, K., Zaragosi, S., Schmidt, F., Rojas, V., and Bassinot, F., 2016, Climatic control of sediment transport from the Himalayas to the proximal NE Bengal Fan during the last glacial-interglacial cycle: *Quaternary Science Reviews*, v. 148, p. 1-16.
- Komar, P.D., 2007. The entrainment, transport and sorting of heavy minerals by waves and currents, *in* Mange, M.A., and Wright, D.T., eds., *Heavy Minerals in Use*: Elsevier, Amsterdam, *Developments in Sedimentology*, v. 58, p. 3-48.
- Kroon, D., Steens, T., and Troelstra, S.R. ,1991, Onset of monsoonal related upwelling in the Western Arabian Sea as revealed by planktonic foraminifers, *in* Prell, W.L., Niitsuma, N., Meyers, P.A., and Emeis, K.K.C., eds., *Proceedings of the Ocean Drilling Program: Scientific Results*, v. 117. College Stations, Texas, p. 257–263.
- Kudrass, H.R., Spiess, V., Bruns, A., Ding, F., Fekete, N., Fenner, J., France-Lanord, C., Palamenghi, L., Reinhardt, L., and Rühlemann, C., et al., 2007, Cruise Report SO 188-2 Chittagong (Bangladesh)—Penang (Malaysia) 06.07. 2006–31.07. 2006. BGR: Hannover, Germany, p. 1-100.
- Kudrass, H.R., Machalett, B., Palamenghi, L., Meyer, I., and Zhang, W., 2018, Sediment transport by tropical cyclones recorded in a submarine canyon off Bangladesh: *Geo-Marine Letters*, v. 38(6), p. 481-496.
- Kuehl, S.A., Allison, M. A., Goodbred, S.L., and Kudrass, H., 2005, The Ganges-Brahmaputra Delta, *in* Giosan, L., and Bhattacharya, J.P., eds., *River Deltas—Concepts, Models, and Examples: Special Publication-SEPM*, v. 83, p. 413-434.
- Lang, K.A., Huntington, K.W., Burmester, R., and Housen, B., 2016, Rapid exhumation of the eastern Himalayan syntaxis since the late Miocene. *Geological Society of American, Bulletin*, v. 128, p. 1403–1422.

- Lavé, J., and Avouac, J. P., 2001, Fluvial incision and tectonic uplift across the Himalayas of central Nepal: *Journal of Geophysical Research: Solid Earth*, v.106(B11), p. 26,561-26,591.
- Lenard, S.J., Lave, J., France-Lanord, C., Aumaitre, G., Bourles, D.L., and Keddadouche, K., 2020, Steady erosion rates in the Himalayas through late Cenozoic climatic changes: *Nature Geoscience*, v. 13(6), p. 448-452.
- Li, P., Zhang, C., Guo, Z., Deng, C., Ji, X., Jablonski, N. G., Wu, H., and Zhu, R., 2019, Clay mineral assemblages in the Zhaotong Basin of southwestern China: Implications for the late Miocene and Pliocene evolution of the South Asian monsoon. *Palaeogeography, Palaeoclimatology, Palaeoecology*, v. 516, p. 90-100.
- Limonta, M., Resentini, A., Carter, A., Bandopadhyay, P.C., and Garzanti, E., 2017, Provenance of Oligocene Andaman sandstones (Andaman–Nicobar Islands): Ganga–Brahmaputra or Irrawaddy derived?: *in* Bandopadhyay, P.C., and Carter, A., eds., *The Andaman–Nicobar Accretionary Ridge: Geology, Tectonics and Hazards: Geological Society of London, Memoir 47(1)*, p. 141-152.
- Limonta, M., Andò, S., Bersani, D., and Garzanti, E., 2022, Discrimination of Clinozoisite–Epidote Series by Raman Spectroscopy: An application to Bengal Fan Turbidites (IODP Expedition 354). *Geosciences*, v. 12(12), p. 442, <https://doi.org/10.3390/geosciences12120442>.
- Lupker, M., France–Lanord, C., Lavé, J., Bouchez, J., Galy, V., Métivier, F., Gaillardet, J., Lartiges, B., and Mugnier, J. L., 2011, A Rouse–based method to integrate the chemical composition of river sediments: Application to the Ganga basin: *Journal of Geophysical Research, Earth Surface*, v. 116(F4), p. 1–24.
- Lupker, M., Blard, P. H., Lavé, J., France-Lanord, C., Leanni, L., Puchol, N., Charreau, J., and Bourlès, D., 2012, ¹⁰Be-derived Himalayan denudation rates and sediment budgets in the Ganga basin: *Earth and Planetary Science Letters*, v. 333, p. 146-156.

- Lupker, M., France-Lanord, C., Galy, V., Lavé, J., and Kudrass, H., 2013, Increasing chemical weathering in the Himalayan system since the Last Glacial Maximum. *Earth and Planetary Science Letters*, v. 365, p. 243-252.
- Lupker, M., Lavé, J., France-Lanord, C., Christl, M., Bourlès, D., Carcaillet, J., Maden, C., Wieler, R., Rahman, M., Bezbaruah, D., and Xiaohan, L., 2017, ^{10}Be systematics in the Tsangpo-Brahmaputra catchment: the cosmogenic nuclide legacy of the eastern Himalayan syntaxis: *Earth Surface Dynamics*, v. 5(3), p. 429-449.
- McNeill, L.C., Dugan, B., Backman, J., Pickering, K.T., Pouderoux, H.F., Henstock, T.J., Petronotis, K., Carter, A., Chemale, F., Jr, Milliken, K.L., Kutterolf, S., Mukoyoshi, H., Chen, W., Kachovich, S., Mitchison, F.L., Bourlange, S., Colson, T.A., Frederik, M.C.G., Guerin, G., Hamahashi, M., House, B.M., Hupers, A., Jeppson, T.N., Kenigsberg, A.R., Kuranaga, M., Nair, N., Owari, S., Shan, Y., Song, I., Torres, M.E., Vannucchi, P., Vrolijk, P.J., Yang, T., Zhao, X., and Thomas, E., 2017, Understanding Himalayan erosion and the significance of the Nicobar Fan: *Earth and Planetary Science Letters*, v. 475, p. 134-142.
- Meigs, A.J., Burbank, D.W., and Beck, R.A., 1995, Middle-late Miocene (> 10 Ma) formation of the Main Boundary thrust in the western Himalaya: *Geology*, v. 23(5), p. 423-426.
- Michels, K.H., Suckow, A., Breitzke, M., Kudrass, H.R., and Kottke, B., 2003, Sediment transport in the shelf canyon “Swatch of No Ground” (Bay of Bengal): *Deep Sea Research Part II: Topical Studies in Oceanography*, v. 50(5), p. 1003-1022.
- Milliken, K.L., 2007, Provenance and diagenesis of heavy minerals, Cenozoic units of the northwestern Gulf of Mexico sedimentary basin, *in* Mange, M.A., and Wright, D.T., eds., *Heavy Minerals in Use: Elsevier, Amsterdam, Developments in Sedimentology*, v. 58, p. 247-261.
- Milliman, J.D., and Meade, R.H., 1983, World-wide delivery of river sediment to the oceans: *The Journal of Geology*, v. 91(1), p. 1-21.

- Mirza, M., 2003, Three recent extreme floods in Bangladesh: a hydro-meteorological analysis: *in* Mirza, M., Dixit, A., Nishateds, A., eds., *Flood Problem and Management in South Asia*: Springer, Dordrecht, p. 35-64.
- Morton, A.C., and Hallsworth, C., 2007, Stability of detrital heavy minerals during burial diagenesis, *in* Mange, M.A., and Wright, D.T., eds., *Heavy Minerals in Use*: Elsevier, Amsterdam, *Developments in Sedimentology*, v. 58, p. 215-245.
- Müller, R.D., Sdrolias, M., Gaina, C. and Roest, W.R., 2008, Age, spreading rates, and spreading asymmetry of the world's ocean crust: *Geochemistry, Geophysics, Geosystems*, 9(4), n°Q04006, doi:10.1029/2007GC001743.
- Myrow, P.M., Hughes, N.C., Derry, L.A., McKenzie, N.R., Jiang, G., Webb, A. A. G., Banerjee, D.M., Paulsen, T.S., and Singh, B.P., 2015, Neogene marine isotopic evolution and the erosion of Lesser Himalayan strata: Implications for Cenozoic tectonic history: *Earth and Planetary Science Letters*, v. 417, p. 142-150.
- Najman, Y., 2006, The detrital record of orogenesis: A review of approaches and techniques used in the Himalayan sedimentary basins: *Earth-Science Reviews*, v. 74(1-2), p. 1-72.
- Najman, Y., Bickle, M., Garzanti, E., Pringle, M., Barfod, D., Brozovic, N., Burbank, D. and Ando, S., 2009, Reconstructing the exhumation history of the Lesser Himalaya, NW India, from a multitechnique provenance study of the foreland basin Siwalik Group: *Tectonics*, v. 28(5), n° TC5018, doi:10.1029/2009TC002506.
- Najman, Y., Bickle, M., Garzanti, E., Pringle, M., Barfod, D., Brozovic, N., Burbank, D., and Andò, S., 2010, Correction to “Reconstructing the exhumation history of the Lesser Himalaya, NW India, from a multitechnique provenance study of the foreland basin Siwalik Group”: *Tectonics*, 29(6), n° TC6006, doi:10.1029/2010TC002778.

- Najman, Y., Mark, C., Barfod, D.N., Carter, A., Parrish, R., Chew, D., and Gemignani, L., 2019, Spatial and temporal trends in exhumation of the Eastern Himalaya and syntaxis as determined from a multitechnique detrital thermochronological study of the Bengal Fan: *Geological Society of America, Bulletin*, v. 131(9-10), p. 1607-1622.
- Odom, I.E., Doe, T.W., and Dott, R.H., 1976, Nature of feldspar-grain size relations in some quartz-rich sandstones: *Journal of Sedimentary Petrology*, v. 46, p. 862-870.
- Pandey, D.K., Clift, P.D., Kulhanek, D.K., and 355 Scientists, Expedition, 2016, Expedition 355 summary. Arabian Sea Monsoon, *in* Pandey, D.K., Clift, P.D., Kulhanek, D.K., Expedition 355 Scientists, eds., *Expedition 355 Scientific Prospectus: Arabian Sea Monsoon. Proceedings of the International Ocean Discovery Program. vol. 355: International Ocean Discovery Program, College Station, Texas*, p. 1–32. <https://doi.org/10.14379/iodp.proc.355.101.2016>.
- Pickering, K.T., Carter, A., Andò, S., Garzanti, E., Limonta, M., Vezzoli, G., and Milliken, K.L., 2020, Deciphering relationships between the Nicobar and Bengal submarine fans, Indian Ocean: *Earth and Planetary Science Letters*, v. 544, n°116329.
- Prell, W.L., and Kutzbach, J.E., 1992, Sensitivity of the Indian monsoon to forcing parameters and implications for its evolution: *Nature* v. 360, p. 647–652.
- Resentini, A., Goren, L., Castellort, S., and Garzanti, E., 2017, Partitioning sediment flux by provenance and tracing erosion patterns in Taiwan: *Journal of Geophysical Research, Earth Surface*, v. 122(7), p. 1430-1454.
- Riad, S., Abdelrahman, E.M., Refai, E., and El-Ghalban, H.M., 1989, Geothermal studies in the Nile Delta, Egypt: *Journal of African Earth Sciences*, v. 9, p. 637–649.
- Sanyal, P., Bhattacharya, S.K., and Prasad, M., 2005, Chemical diagenesis of Siwalik sandstone: isotopic and mineralogical proxies from Surai Khola section, Nepal, *Sedimentary Geology*, v. 180 (1-2), p. 57-74.

- Schwenk, T., and Spieß, V., 2009, Architecture and stratigraphy of the Bengal Fan as response to tectonic and climate revealed from high-resolution seismic data, *in* Kneller, B., Martinsen, O.J., and McCaffrey, B., External Controls on Deep-Water Depositional Systems: SEPM (Society for Sedimentary Geology) Special Publication 92, p. 107-131.
- Sciunnach, D., and Garzanti, E., 2012, Subsidence history of the Tethys Himalaya: *Earth-Science Reviews*, v. 111(1-2), p. 179-198.
- Sharp, J.M., Galloway, W.E., Land, L.S., McBride, E.F., Blanchard, P.E., Bodner, D.P., Dutton, S.P., Farr, M.R., Gold, P.B., Jackson, T.J., Lundegard, P.D., Macpherson, G.L., and Milliken, K.L., 1988, Diagenetic processes in Northwest Gulf of Mexico sediments, *in* Chilingarian, G.V., and Wolf, K.H., eds., *Diagenesis II: Developments in Sedimentology Series 43* Elsevier, Amsterdam, pp. 43–133.
- Singh, S.K., and France-Lanord, C., 2002, Tracing the distribution of erosion in the Brahmaputra watershed from isotopic compositions of stream sediments: *Earth and Planetary Science Letters*, v. 202(3-4), p. 645-662.
- Spiess, V., Hübscher, C., Breitzke M., Böke, W., Krell, A., von Larcher, T., Matschkowski, T., Schwenk, T., Wessels, A., Zühlsdorff, L., and Zühlsdorff, S., 1998, Report and preliminary results of R/V Sonne Cruise 125, Cochin-Chittagong, 17.10–17.11.97: [der] Universität Bremen, Berichte aus dem Fachbereich Geowissenschaften 123. <http://elib.suub.uni-bremen.de/ip/docs/00010242>.
- Steinke, S., Mohtadi, M., Groeneveld, J., Lin, L.C., Löwemark, M.C., and Rendle-Bühning, R., 2010, Reconstructing the southern South China Sea upper water column structure since the Last Glacial Maximum: Implications for the East Asian winter monsoon development: *Paleoceanography* v. 25, n°PA2219.
- Szulc, A.G., Najman, Y., Sinclair, H.D., Pringle, M., Bickle, M., Chapman, H., Garzanti, E., Andò, S., Huyghe, P., Mugnier, J.L. and Ojha, T., 2006, Tectonic evolution of the Himalaya constrained

by detrital ^{40}Ar – ^{39}Ar , Sm–Nd and petrographic data from the Siwalik foreland basin succession, SW Nepal: *Basin Research*, v. 18(4), p.375-391.

Thompson, R.W., 1974. Mineralogy of sands from the Bengal and Nicobar fans, Sites 218 and 211, Eastern Indian Ocean: Initial Reports of the Deep Sea Drilling Project: Washington, D.C., U.S. Government Printing Office, v. 22 p. 711-713.

Upadhyay, D., Kooijman, E., Singh, A.K., Mezger, K., and Berndt, J., 2015, The basement of the Deccan Traps and its Madagascar connection: constraints from xenoliths. *The Journal of Geology*, v. 123(3), p. 295-307.

Velbel, M.A., 2007, Surface textures and dissolution processes of heavy minerals in the sedimentary cycle: examples from pyroxenes and amphiboles, *in* Mange, M.A., and Wright, D.T., eds., *Heavy Minerals in Use: Elsevier, Amsterdam, Developments in Sedimentology*, v. 58, p. 113-150.

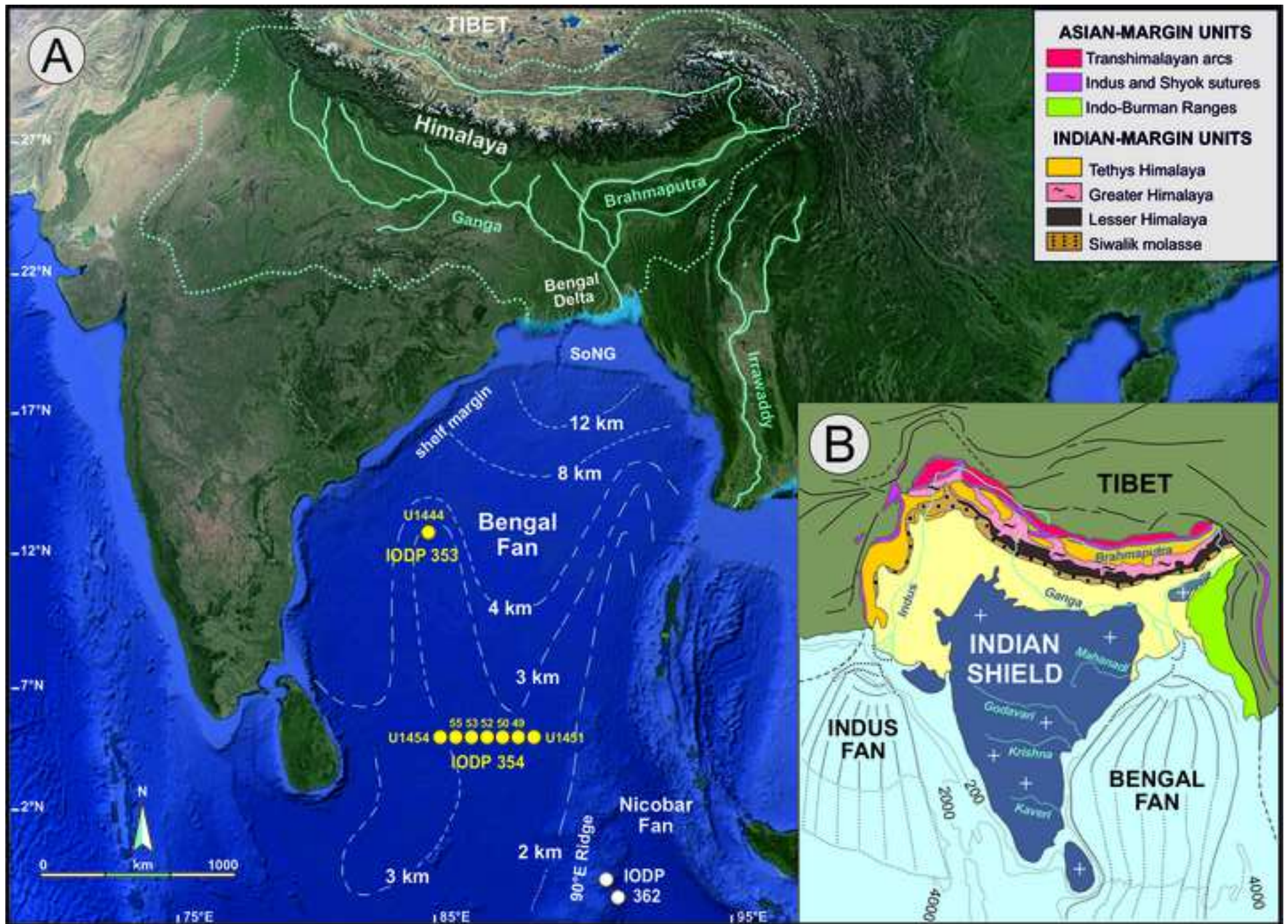
Vögeli, N., Huyghe, P., Van der Beek, P., Najman, Y., Garzanti, E. and Chauvel, C., 2018, Weathering regime in the Eastern Himalaya since the mid–Miocene: Indications from detrital geochemistry and clay mineralogy of the Kameng River Section, Arunachal Pradesh, India: *Basin Research*, v. 30(1), p. 59-74.

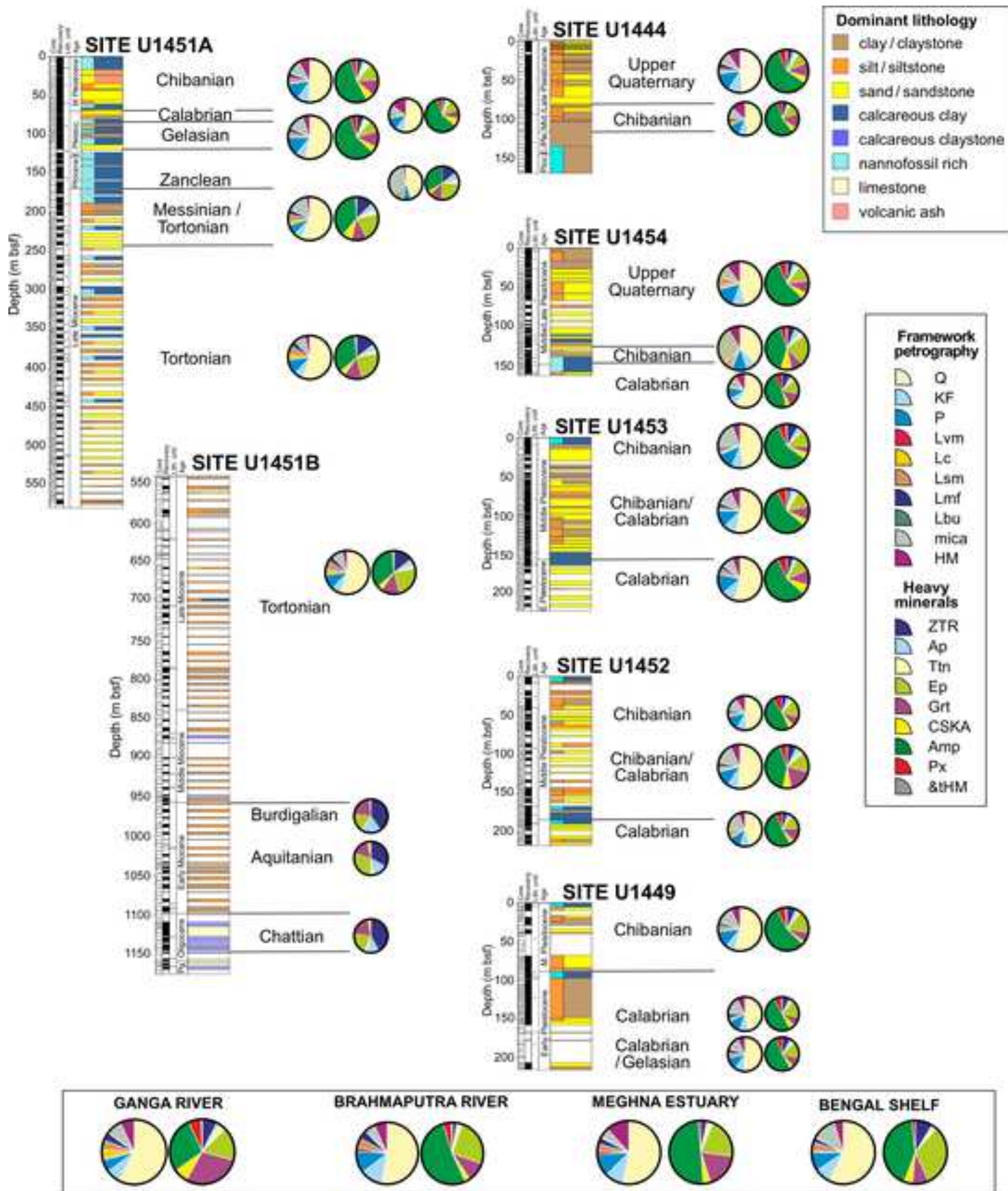
Wang, J.-G., Hu, X.M., Garzanti, E., An, W., and Liu, X.C., 2017, The birth of the Xigaze forearc basin in southern Tibet: *Earth and Planetary Science Letters*, v. 465, p. 38–47.

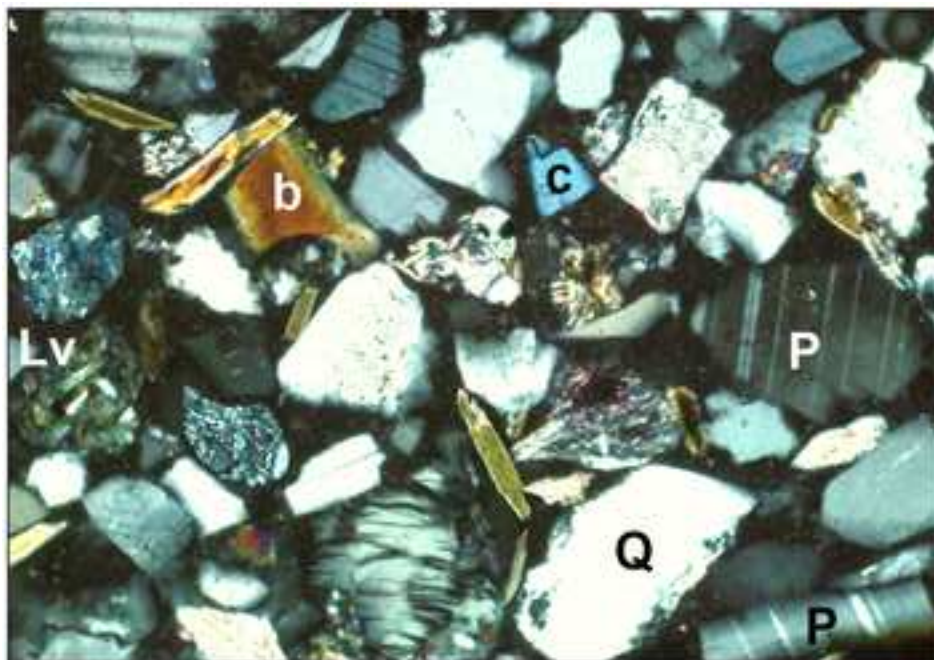
Weber, M.E., and Reilly, B.T., 2018, Hemipelagic and turbiditic deposits constrain lower Bengal Fan depositional history through Pleistocene climate, monsoon, and sea level transitions: *Quaternary Science Reviews*, v. 199, p.159-173.

Weltje, G.J., 1997, End-member modeling of compositional data: Numerical-statistical algorithms for solving the explicit mixing problem: *Mathematical Geology*, v. 29(4), p. 503-549.

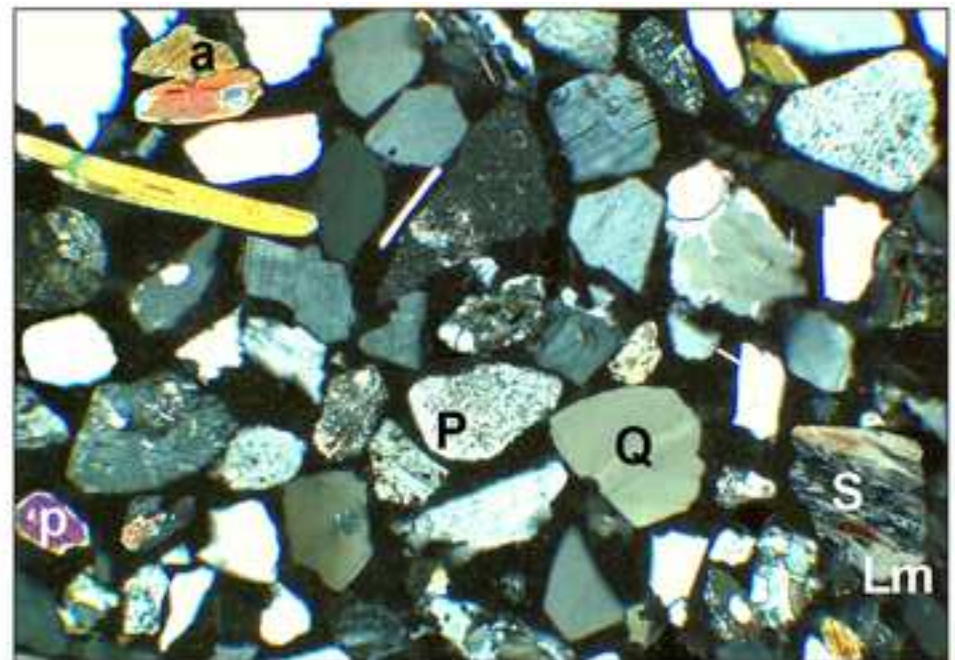
- White, N.M., Pringle, M., Garzanti, E., Bickle, M., Najman, Y., Chapman, H. and Friend, P., 2002, Constraints on the exhumation and erosion of the High Himalayan Slab, NW India, from foreland basin deposits: *Earth and Planetary Science Letters*, v. 195(1-2), p. 29-44.
- Yokoyama, K., Amano, K., Taira, A., and Saito, Y., 1990, Mineralogy of silts from the Bengal Fan: *Proceedings of the Ocean Drilling Program, Scientific Results*, v. 116, p. 59– 73.
- Yoshida, K., Nakajima, T., Matsumoto, Y., Osaki, A., Rai, L.K., Cruz, J.W., and Sakai, H., 2021, Miocene provenance change in Himalayan foreland basin and Bengal Fan sediments, with special reference to detrital garnet chemistry: *Island Arc*, v. 30(1), n° e12408.
- Zeitler, P.K., Meltzer, A.S., Koons, P.O., Craw, D., Hallet, B., Chamberlain, C.P., Kidd, W.S., Park, S.K., Seeber, L., Bishop, M., and Shroder, J., 2001, Erosion, Himalayan geodynamics, and the geomorphology of metamorphism: *GSA Today*, v. 11(1), p.4-9.
- Zhang, P., Najman, Y., Mei, L., Millar, I., Sobel, E.R., Carter, A., Barfod, D., Dhuime, B., Garzanti, E., Govin, G. and Vezzoli, G., 2019, Palaeodrainage evolution of the large rivers of East Asia, and Himalayan-Tibet tectonics: *Earth-Science Reviews*, v. 192, p. 601-630.
- Zheng, H.B., Powell, C.M., An, Z.S., Zhou, J., and Dong, G., 2000, Pliocene uplift of the northern Tibetan Plateau: *Geology* v. 28, p. 715–718.
- Zhu, D.C., Zhao, Z.D., Niu, Y.L., Mo, X.X., Chung, S.L., Hou, Z.Q., Wang, L.Q., and Wu, F.Y., 2011, The Lhasa terrane: Record of a microcontinent and its histories of drift and growth. *Earth and Planetary Science Letters*, v. 301, p. 241–255.
- Zuffa, G.G., 1985; Optical analyses of arenites: influence of methodology on compositional results, *in* Zuffa, G.G., ed., *Provenance of Arenites*: Reidel Publishing Company, Dordrecht, NATO ASI Series C 148, p. 165-189.



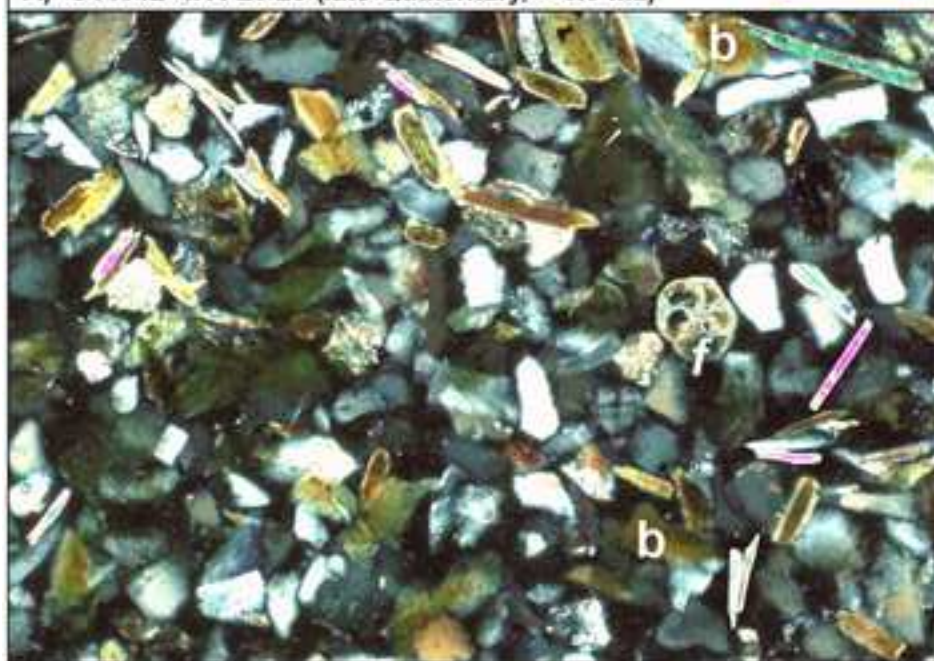




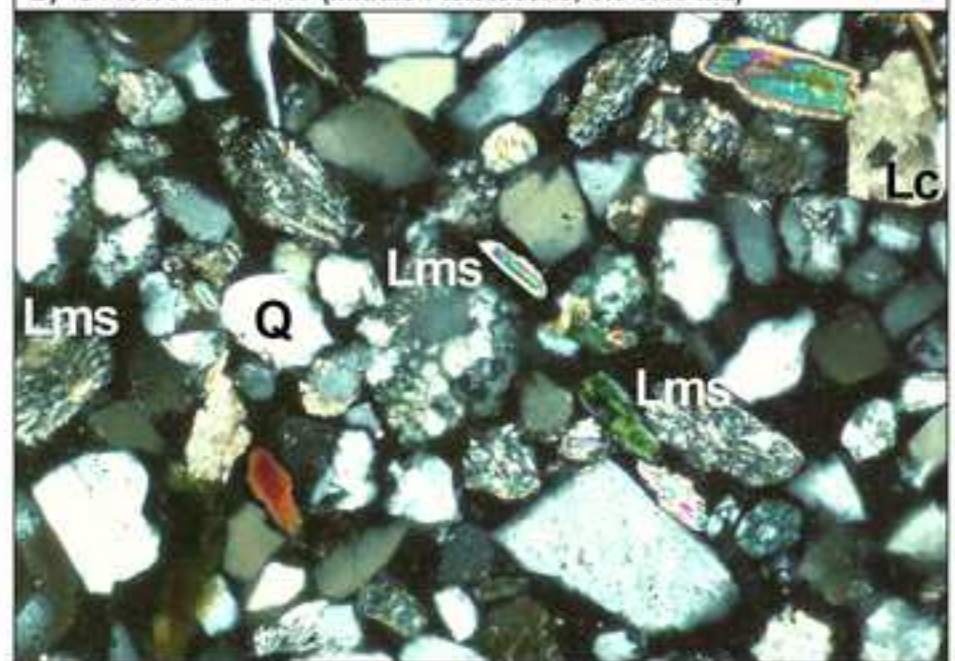
A) U1454B 4H4 20-25 (late Quaternary, < 0.3 Ma)



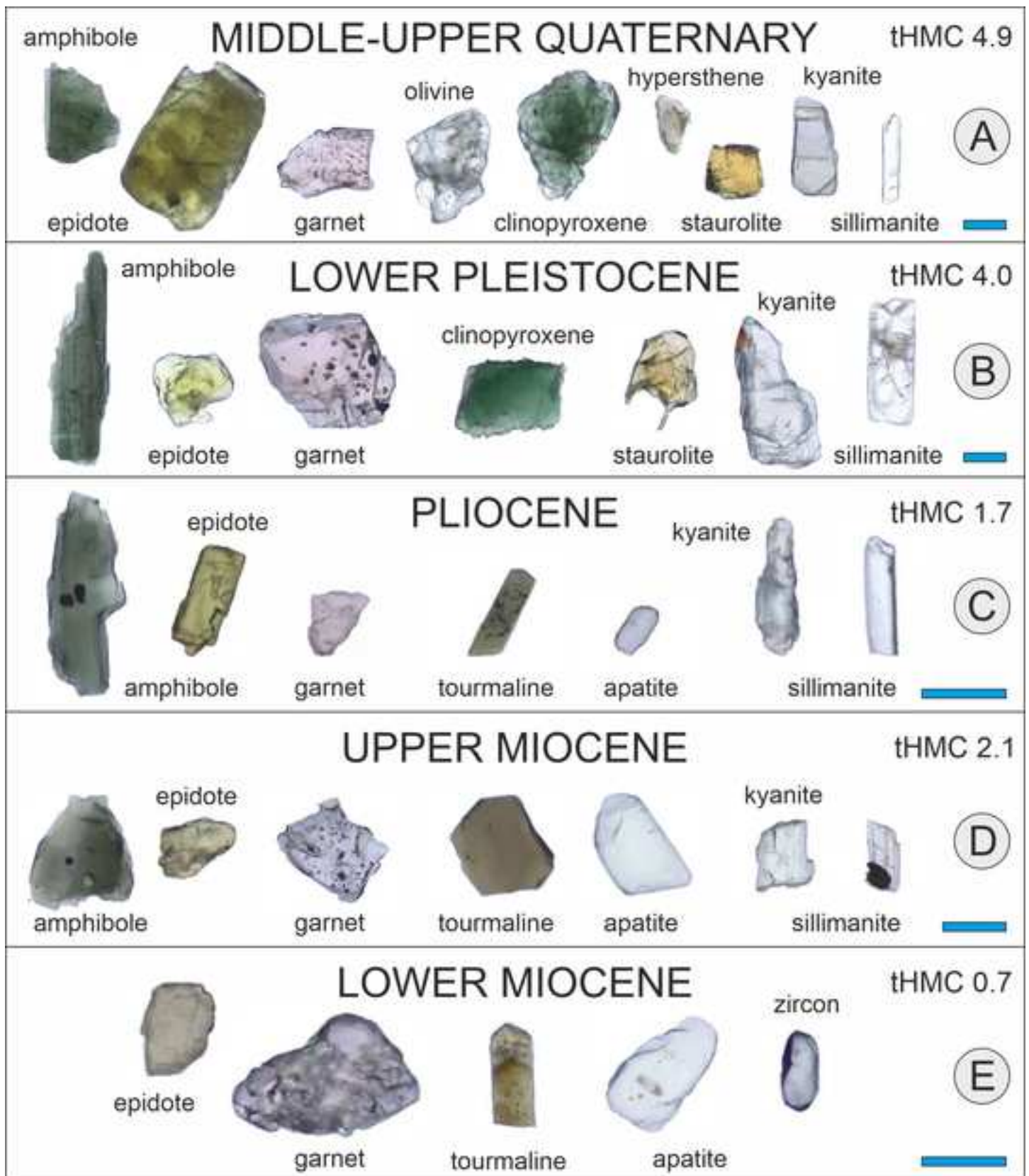
B) U1451A 7H1 10-15 (Middle Pleistocene, 0.3-0.45 Ma)

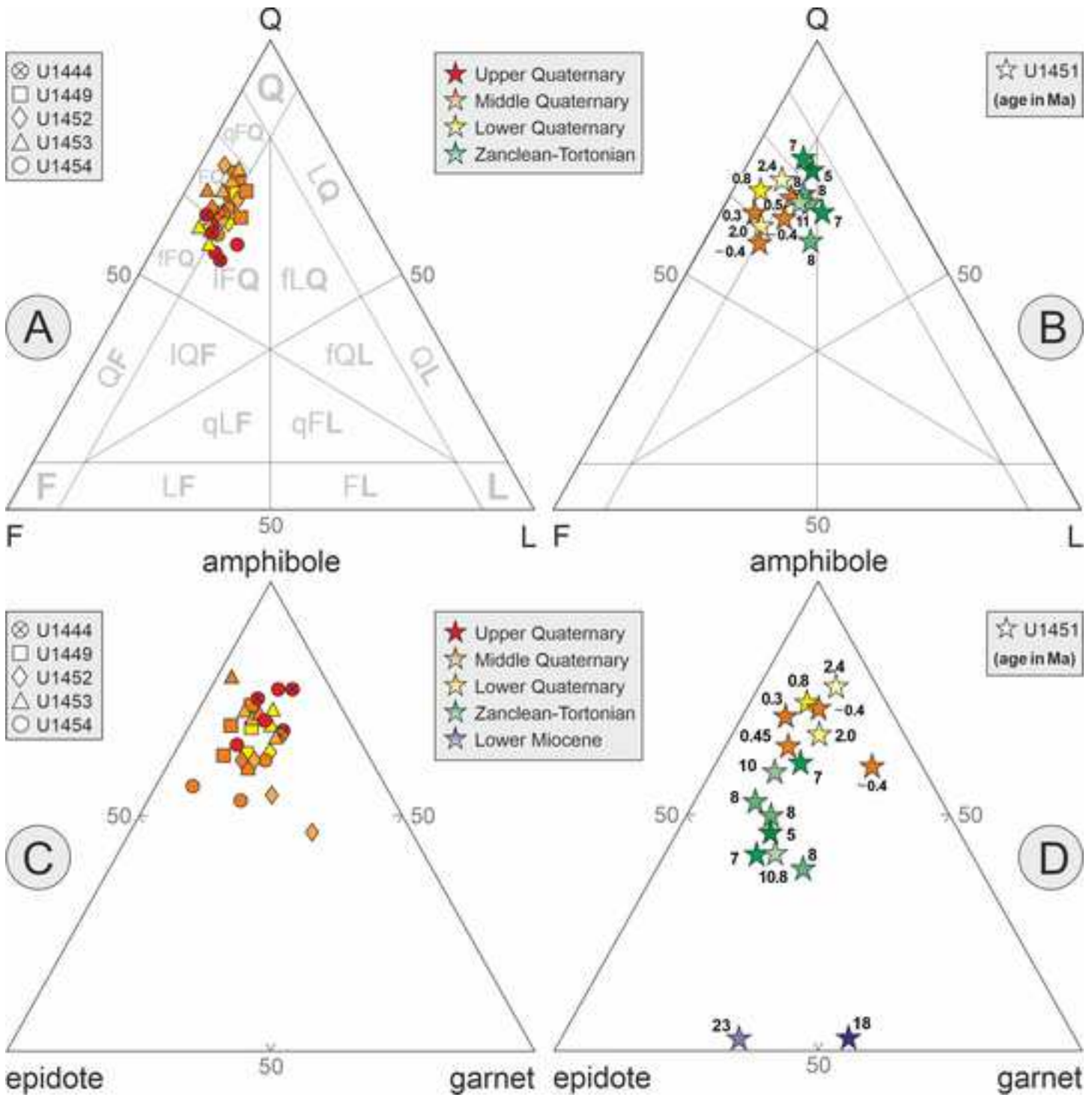


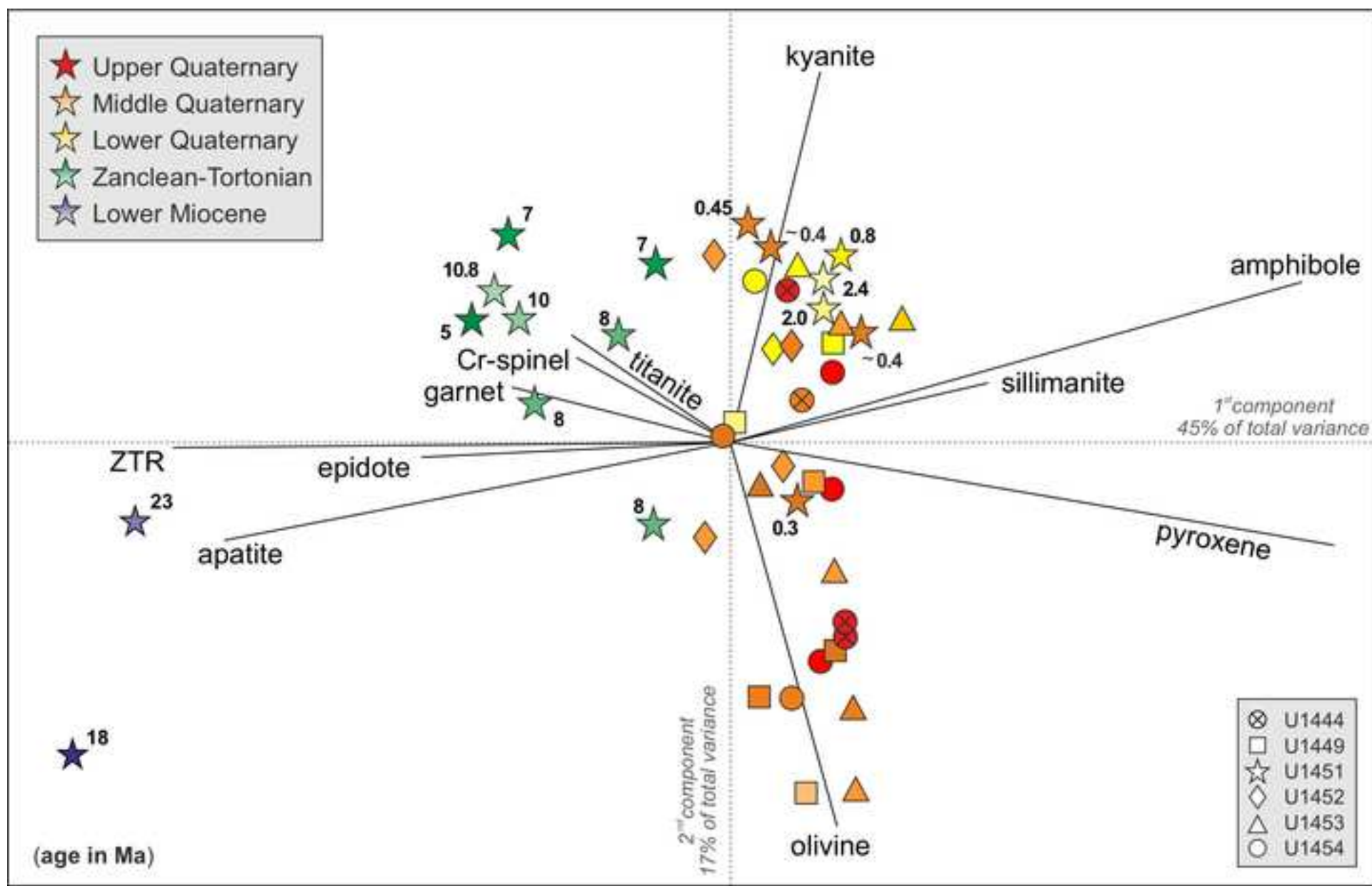
C) U1451A 27H2 25-30 (Zanclean, 5 Ma)

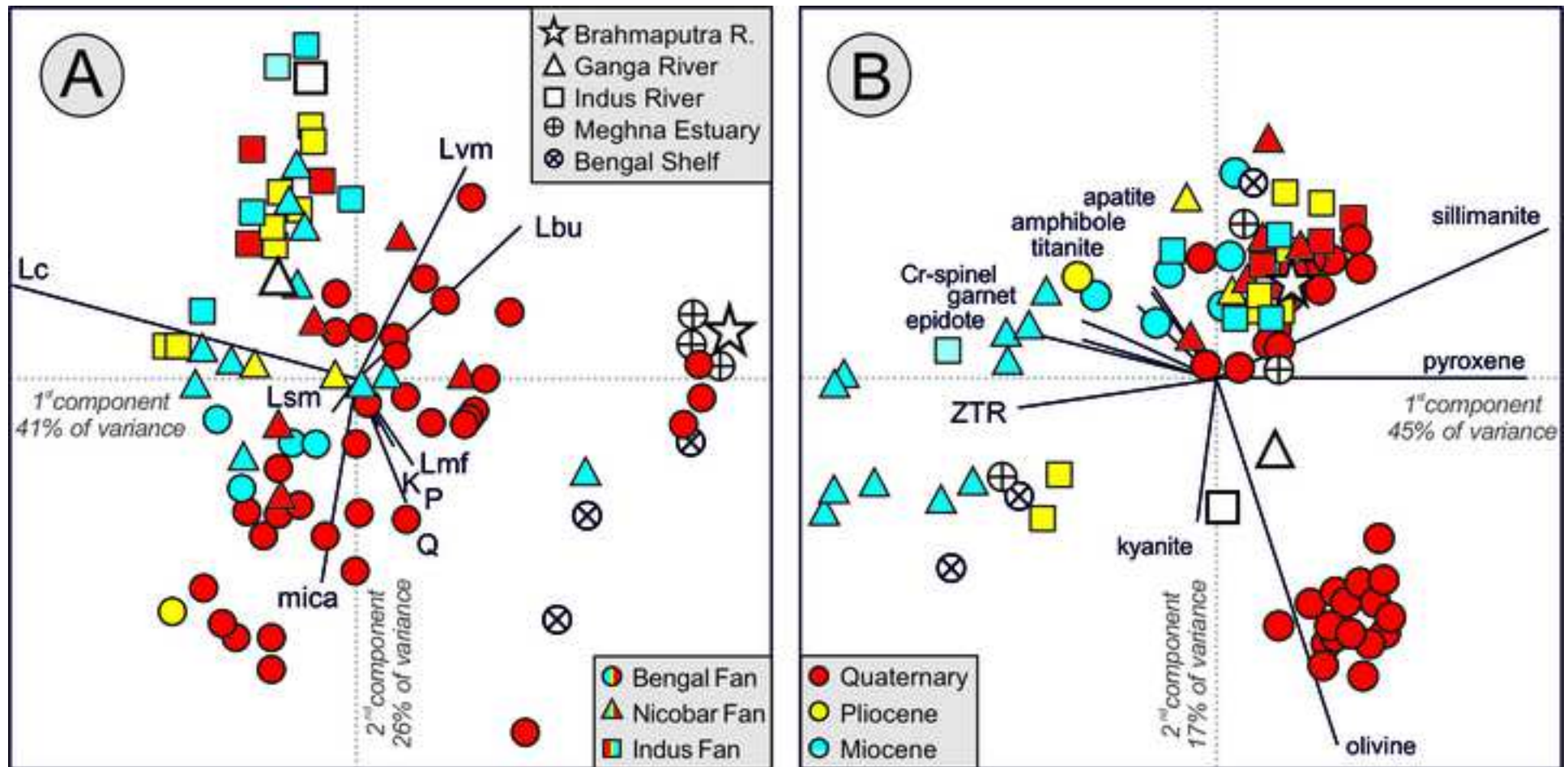


D) U1451A 74F4 85-80 (Tortonian, 8 Ma)






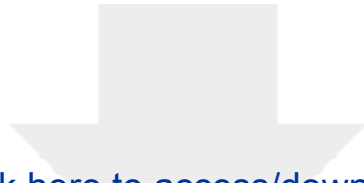




Expedition	Hole	Latitude (N)	Longitude (E)	Water depth (m)	Core interval (m)	Recovery (%)	Age	n° samples
353	U1444A	14°0.0057	84°49.7405	3143	330.6	68.0%	Miocene-recent	4
354	U1454B	8°0.4083	85°51.0025	3710	147.4	91.1%	Calabrian-recent	6
354	U1453A	8°0.4193	86°47.8973	3680	186.7	86.6%	Calabrian-Chibanian	7
354	U1452B	8°0.4191	87°10.9128	3670	174.5	80.2%	Calabrian-Chibanian	5
354	U1449A	8°0.4194	88°65.9994	3653	212.5	99.5%	Calabrian-Chibanian	6
354	U1451A	8°0.4195	88°44.5012	3607	394.9	67.8%	Tortonian-Chibanian	15
354	U1451B	8°0.4203	88°44.4745	3607	627.6	53.1%	Oligocene	3

Table2 [Click here to access/download;Table;Bengal PTHM Table 2.xls](#) 

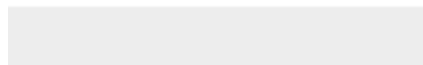
Unit	N°	Q	KF	P	Lc	&Lsm	Lmf	Lvbu	mica	HM	total	MI	ZTR	Ap	Ttn	Ep	Grt	CSKA	Amp	Px	&tHM	total	tHMC	G/GCSKA		
MODERN SANDS																										
Ganga River °	7	58	7	6	5	5	4	1	8	7	100.0	250	7	2	3	17	29	7	28	6	0.5	100.0	9.0	81		
Brahmaputra River °	6	53	12	12	0.2	5	5	3	5	7	100.0	256	2	1	2	25	10	3	52	4	0.5	100.0	10.4	79		
Meghna Estuary °	3	53	9	11	0.3	4	3	2	5	12	100.0	250	3	1	3	21	18	4	50	1	0	100.0	13.7	83		
Bengal Shelf °	3	57	8	9	0.1	5	2	1	12	5	100.0	207	9	1	2	32	8	4	42	2	0	100.0	7.4	66		
Indus River °	8	41	9	10	9	9	4	4	3	9	100.0	214	3	1	2	25	12	3	50	4	0.1	100.0	8.0	79		
Indus Delta §	9	40	9	12	8	5	4	3	16	2	100.0	212	3	1	2	27	6	3	52	6	0.1	100.0	2.6	64		
BENGAL FAN																										
Quaternary U1444 *	4	48	10	13	1	3	4	0.6	10	10	100.0	266	5	3	2	10	12	5	58	6	0.6	100.0	5.9	70		
Quaternary U1454 *	6	45	8	13	1	2	4	1	15	10	100.0	263	6	3	3	17	10	6	49	6	0.5	100.0	6.3	63		
Quaternary U1453 *	7	52	9	13	0.5	2	3	1	13	7	100.0	239	5	3	2	12	9	5	57	7	0.5	100.0	3.8	63		
Quaternary U1452 *	5	50	9	12	2	2	3	0.5	15	7	100.0	255	6	4	3	15	15	6	44	6	0.2	100.0	4.8	73		
Quaternary U1449 *	6	51	8	12	0.6	3	3	1	14	7	100.0	254	7	3	2	17	8	4	52	6	1	100.0	3.5	69		
Quaternary U1451 *	7	52	8	13	1	3	3	0.5	11	8	100.0	247	5	2	4	12	12	6	56	4	0.3	100.0	4.0	67		
Mio-Pliocene (3-8 Ma) *	3	52	5	7	3	5	3	0.4	22	2	100.0	211	13	6	4	22	12	6	36	0.3	0.2	100.0	1.8	66		
Tortonian (8-11 Ma) *	5	56	7	11	4	7	4	0.4	8	4	100.0	224	13	5	3	25	13	4	37	1	0.3	100.0	1.7	77		
Oligo-Mioc.(18-28 Ma) *	3	n.d.	n.d.	n.d.	n.d.	n.d.	n.d.	n.d.	n.d.	n.d.		n.d.	38	15	2	23	19	2	0.3	0	0.3	100.0	0.6	91		
NICOBAR FAN																										
Quaternary #	5	55	8	12	2	3	3	1	13	3	100.0	254	4	4	2	17	16	5	50	3	0	100.0	4.6	77		
Mio-Pliocene (3-8 Ma) #	3	70	8	7	1	2	2	1	6	3	100.0	224	8	4	1	21	11	3	51	1	0.2	100.0	3.1	77		
Tortonian (8-11 Ma) #	10	55	6	7	4	9	4	1	12	2	100.0	172	11	7	2	37	14	3	25	0.05	0.1	100.0	1.9	82		
INDUS FAN																										
Quaternary °	4	40	7	10	10	7	3	2	19	3	100.0	188	1	3	2	26	5	4	53	5	0.6	100.0	5.8	57		
Mio-Pliocene (3-8 Ma) °	12	44	7	14	8	7	3	3	10	4	100.0	184	2	2	2	28	6	3	50	6	1	100.0	6.5	67		
Miocene (14-18 Ma) °	1	40	6	13	16	9	3	5	4	3	100.0	160	5	2	2	49	5	1	33	1	2	100.0	2.6	79		



Click here to access/download

Supplemental Material

Bengal PTHM Appendix A Captions.docx

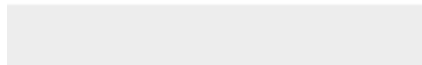


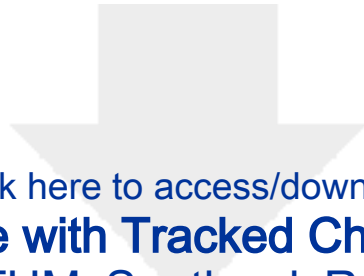


Click here to access/download

Supplemental Material

Bengal PTHM Appendix A Tables.xls





[Click here to access/download](#)

Article with Tracked Changes

[Limonta&BengalPTHM_Southard_RevisionMarked.docx](#)

